



OPEN ACCESS

EDITED BY

Hu Li,
Sichuan University of Science and
Engineering, China

REVIEWED BY

Wei Ju,
China University of Mining and
Technology, China
Jingshou Liu,
China University of Geosciences
Wuhan, China

*CORRESPONDENCE

Kun Dai,
✉ daikundr@163.com
Yan Xia,
✉ xiayandr@163.com
Haowei Yuan,
✉ kangjihao2025666@163.com

RECEIVED 22 November 2025

REVISED 07 January 2026

ACCEPTED 08 January 2026

PUBLISHED 24 February 2026

CITATION

Dai K, Xia Y, Liu T, Zhang H, Fu P, Yuan H,
Ren S and Liu C (2026) Geochemical and
geophysical constraints on deep fluid
activities in sedimentary basins: a study of
Jimsar Sag in Junggar Basin.
Front. Earth Sci. 14:1751788.
doi: 10.3389/feart.2026.1751788

COPYRIGHT

© 2026 Dai, Xia, Liu, Zhang, Fu, Yuan, Ren and
Liu. This is an open-access article distributed
under the terms of the [Creative Commons
Attribution License \(CC BY\)](https://creativecommons.org/licenses/by/4.0/). The use,
distribution or reproduction in other forums is
permitted, provided the original author(s) and
the copyright owner(s) are credited and that
the original publication in this journal is cited,
in accordance with accepted academic
practice. No use, distribution or reproduction
is permitted which does not comply with
these terms.

Geochemical and geophysical constraints on deep fluid activities in sedimentary basins: a study of Jimsar Sag in Junggar Basin

Kun Dai^{1,2*}, Yan Xia^{1,2*}, Tianen Liu^{1,2}, Hong Zhang^{1,2}, Pan Fu^{1,2},
Haowei Yuan^{3,4*}, Shiju Ren^{1,2} and Chang Liu^{1,2}

¹CNPC Engineering Technology R&D Company Limited, Beijing, China, ²National Engineering Research Center of Oil & Gas Drilling and Completion Technology, Beijing, China, ³National Key Laboratory of High-Efficiency Flexible Coal Power Generation and Carbon Capture Utilization and Storage, Beijing, China, ⁴China Huaneng Clean Energy Research Institute, Beijing, China

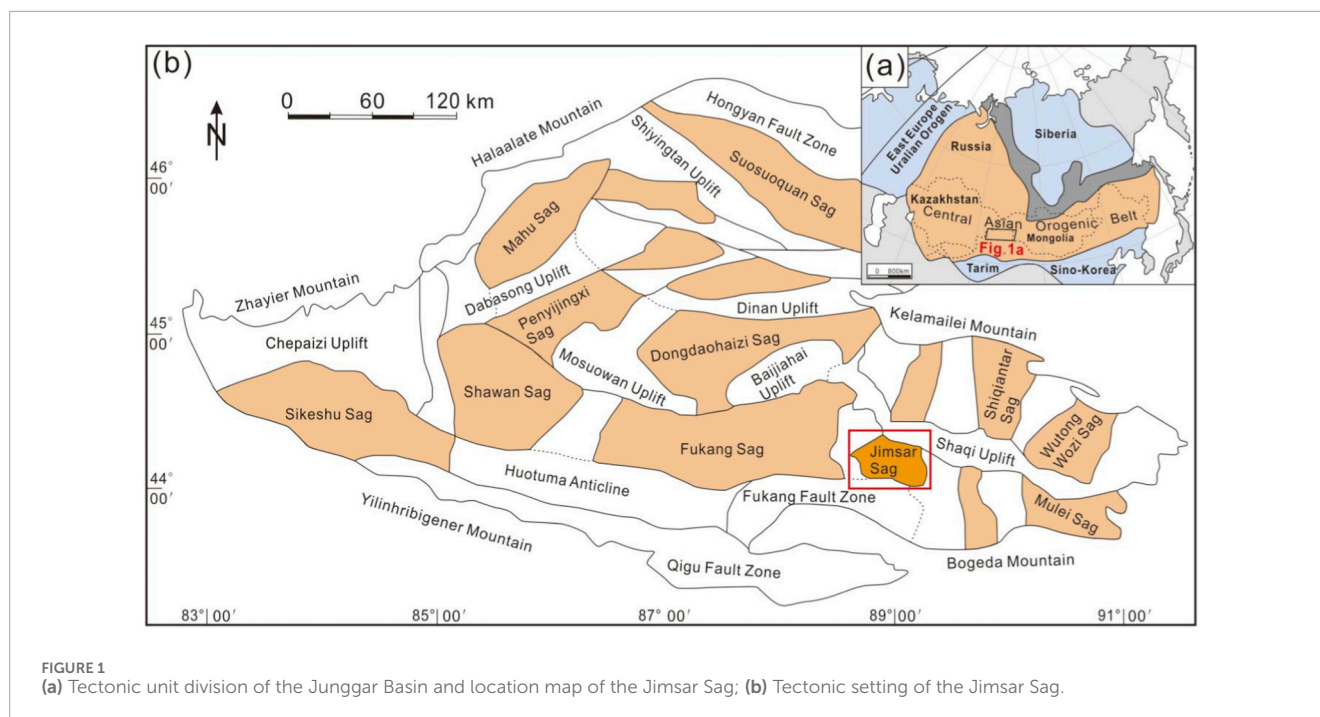
Deep fluids of the Earth are characterized by their unique physical and chemical properties, and they play important roles in various geological processes. Despite the importance of Earth's aqueous fluids in sedimentary basins, few techniques are currently available to directly trace their origins, especially for those in the deep mantle and lower crust. In this study, we report data about fluid fillings in forms of calcites in the fractures of the Jimsar Sag, Junggar Basin, including their trace elements, Nd-C-O isotopes, Sm-Nd isochron ages and fluid inclusion features. According to comprehensive analyses of rock acoustic emission and joint rose statistics, we suggest that there are mainly three episodes of tectonic-fluid activities. As indicated by the Sm-Nd isochron ages, NW tensile fractures and NEE shear fractures in the Jimsar Sag are filled by mantle magmatism- and lower crust magmatism-related fluids at 272.4 Ma and 189.5 Ma, respectively. Subsequently, the third episode of fluid filling occurs in the NNW shear fractures at 124.3 Ma. Specifically, we emphasize that geophysical and geochemical methods should be combined to collectively constrain research on fluid activity episodes and fluid origins. Moreover, constraint on fluid activities in the deep Earth also relies on combination with regional tectonic evolution history and magmatism characteristics.

KEYWORDS

calcites, deep mantle and lower crust, Jimsar Sag, Junggar Basin, tectonic-fluid activities

1 Introduction

As a dominant factor controlling material evolution and energy redistribution in the sedimentary basins, fluids are extensively involved in the tectonic, sedimentary, diagenetic and mineralizing processes (Walter et al., 1990; Kent et al., 2002; Anderson et al., 2004; Staudigel et al., 2018). Previous studies on basin fluids mainly highlight atmospheric gas, fresh water of meteoric origin, lake water, seawater, mixed water, evaporated water, oil, and natural gas, with little attention paid to magmatism-related deep fluids



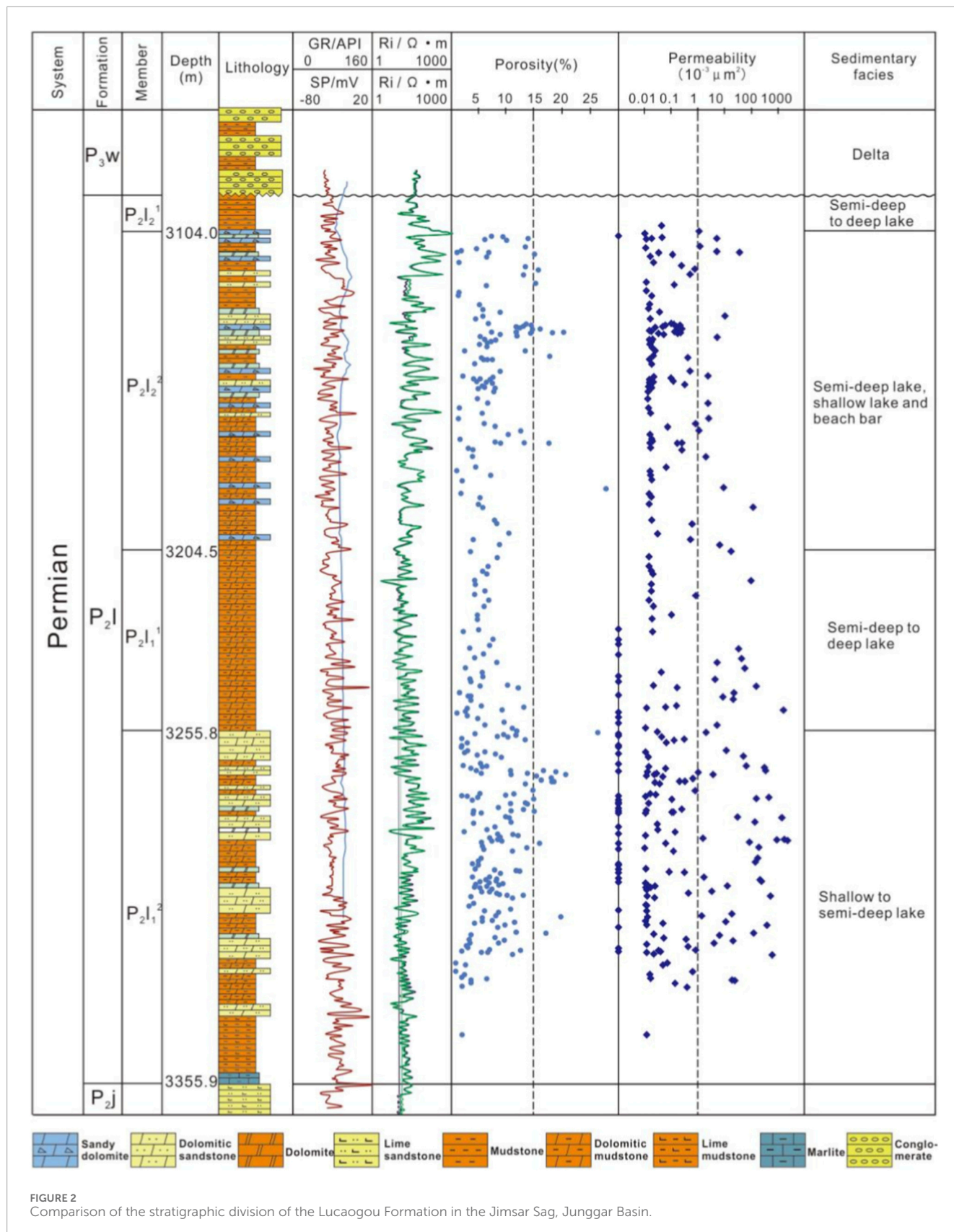
(Stasiuk and Snowdon, 1997; Goldstein, 2001; Immerzeel et al., 2015; Staudigel et al., 2018; Agrinier et al., 2019). In sedimentary basins, sedimentation sometimes coincides or alternates with volcanic-magmatic activities, accompanied by invasion of magmatic rocks and entrance of deep fluid matter in different forms into the basin (Sibuet et al., 1998; Hergt and Woodhead, 2007; Keith et al., 2017). Specifically, tectonic deformation and/or physical diagenesis can lead to formation of weak planes at different scales in the continental crust, ranging from the fracture scale to the deep fault scale, which collectively act as channels for deep matter to enter into sedimentary basins (Ruch et al., 2016; Montanari et al., 2017; Dering et al., 2019). Deep fluids are important components of deep matter, and they are also important carriers of deep energy and matter. Moreover, they are a crucial link between internal and external factors in the basin (Hazen and Schiffries, 2013). Rifting-related basins are typically characterized by coexistence of sedimentary rocks, volcanic rocks and intrusive rocks, as well as deep faults that favor deep fluid activities (Hadlari et al., 2016; Smets et al., 2016; Hart et al., 2017; Elliott et al., 2017).

Deep fluids are generally defined as matter that can flow in the deep Earth, including gases, liquids, and plastic fluids (Goyal et al., 2016; Kietäväinen et al., 2017; Telling et al., 2018). Magmatism-related deep fluids are usually of crustal and mantle origins (Jin et al., 2017). Among them, most crustal fluids originate from ancient strata in the deep basin, partly from the crystallization basement, and they are in many cases mixed with each other (Shankland and Ander, 1983; Stuart et al., 1995; Sibson, 1994; Markl and Bucher, 1998; Balfour et al., 2015; Hu et al., 2016). Activities of some crustal fluids are demonstrated to be associated with specific volcanic-magmatic events, and they are thought to be thermal fluid activities triggered by magmatic heating in the deep

basin (Peacock et al., 2015; Gao et al., 2016; Seewald et al., 2019). In comparison, mantle fluids are attributable to thermal fluid activities induced by crustal magmatism (Jin et al., 2017; Hu et al., 2016).

Favored by their relatively high solubility in fluids, Sr isotopes are generally used for fluid activity analysis (Foden et al., 2001; Grandia et al., 2003; Stewart et al., 2015). However, Sr is a relatively mobile element in aqueous fluids, compared with other elements such as Nd and Hf (Woodhead et al., 2001; Kessel et al., 2005; Turner et al., 2009). Therefore, large uncertainty exists when Sr is used to trace fluid origin. For instance, felsic clastic rocks and mudstones in the sedimentary basins usually contain more radioactive ^{87}Sr , which results in overall high $^{87}\text{Sr}/^{86}\text{Sr}$ ratios (Winter et al., 1997). Meanwhile, the reaction between atmospheric precipitation and debris matter on the ground surface can also lead to high $^{87}\text{Sr}/^{86}\text{Sr}$ ratios. In this context, these high $^{87}\text{Sr}/^{86}\text{Sr}$ ratios might overprint the initial $^{87}\text{Sr}/^{86}\text{Sr}$ signatures of magmatism-related deep hydrothermal fluids during their upward migration along the fault (Zhu et al., 2013). Therefore, more precise methods are needed to constrain origin and activity rules of both shallow and deep fluids.

With strong migration capacity, fluids are usually in forms of fracture fillings. In this study, we investigate fluid features and activity rules in the fracture fillings of the Permian Lucaogou Formation, Jimsar Sag, Junggar Basin, China, where fluid activities are relatively strong, through characterization of their trace elements, Nd-C-O isotopes, Sm-Nd isochron ages and fluid inclusion. Moreover, regional tectonic evolution that influences fracture development is combined to elaborate the relationship between tectonic evolution and fluid activity in the Jimsar Sag, Junggar Basin.



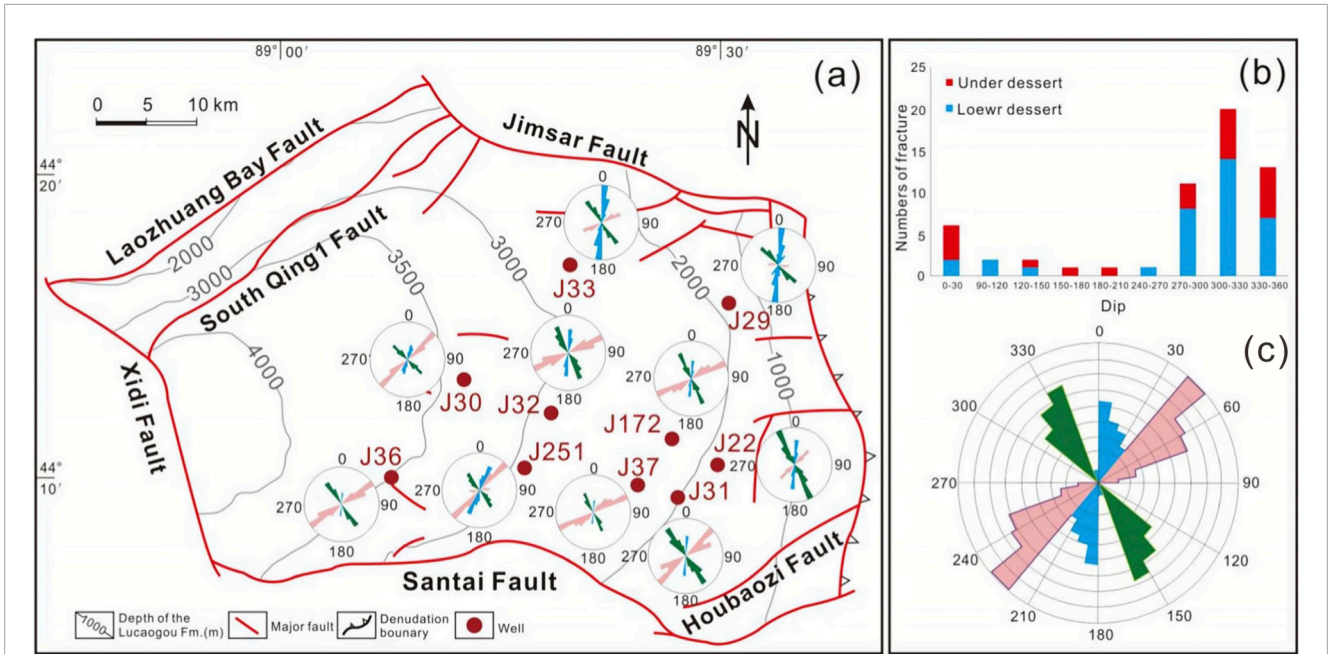


FIGURE 3 Imaging logging-based statistics on fractures in Wells J33, J29, J30, J36, J32, J251, J172, J37, J22, and J31. **(a)** rose diagram for joint strikes in single wells; **(b)** rose diagram for joint dip angles in single wells; **(c)** rose diagram for joint strikes of all wells.

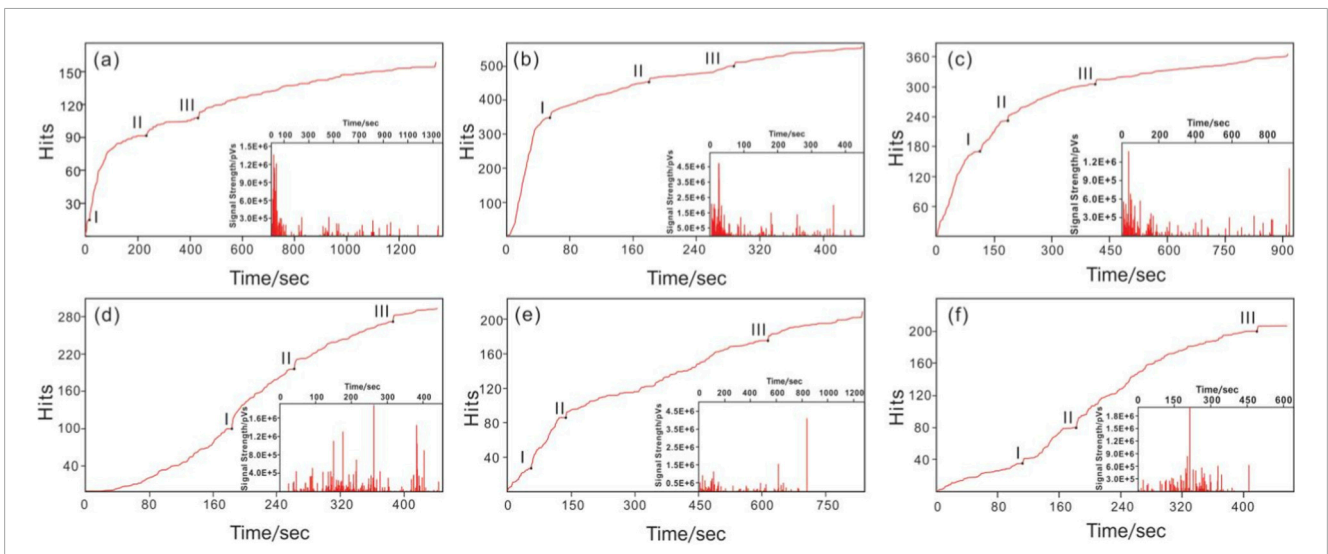
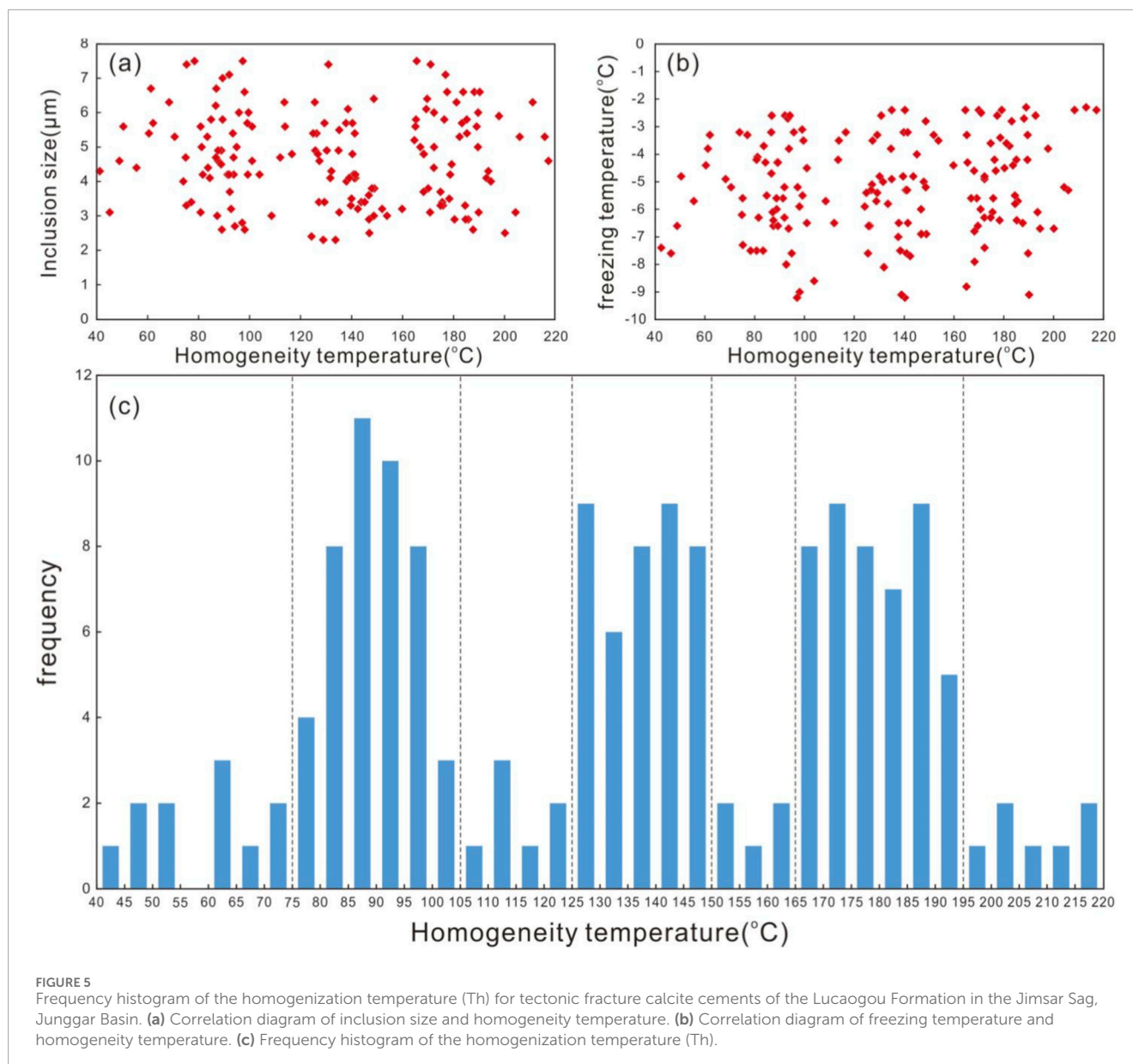


FIGURE 4 Acoustic emission (AE) curve of the Lucaogou Formation in the Jimsar Sag, Junggar Basin. **(a)** J32 well, 3570.5 m; **(b)** J32 well, 3681.5; **(c)** J174 well, 3154.8 m; **(d)** J174 well, 3266.9; **(e)** J176 well, 3029.4 m; **(f)** J176 well, 3046.2 m.

2 Geological setting

Located in the southern part of the Central Asian Orogenic Belt and in the north of Xinjiang, the Junggar Basin is triangularly sandwiched between the Tianshan Orogenic Belt in the south, the Altai Orogenic Belt in the northeast, and the Zaire and Halalalat

Mountains in the northwest. As a Mesozoic-Cenozoic sedimentary basin that develops on the Paleozoic basement, the basin is underlain by Precambrian crystalline and slightly metamorphosed Paleozoic basement units (Zhang et al., 1999), and records the evolution from a Paleozoic foreland basin to a Mesozoic fault-depression basin, and finally a Cenozoic foreland Basin. The Jimsar Sag is located



in the southeastern part of the Junggar Basin (Figure 1a), and it is bounded by the Jimsar Fault in the north, the Santai Fault in the south, the Laozhuangwan and Xidi Faults in the west, and the Qitai Uplift in the east. It is basically a half graben-like sag with a deeper, faulted western part and a shallower, overlapped eastern part, covering an area of about 1,278 km² (Figure 1b). Developing on the Lower Carboniferous fold basement, there are only relatively weak tectonic activities in the Jimsar Sag, accompanied by consequent relatively complete sedimentary strata from the Permian to the Quaternary, with a maximum thickness of more than 5,000 m.

Distributed throughout the Jimsar Sag, the Permian Lucaogou Formation is generally thick in the south and west while thin in the north and east, with an average thickness of 200–350 m. There are mainly two fining-upward sequences from bottom

to top corresponding to two sandstone-mudstone reservoir-cap assemblages, namely, the first member of the Lucaogou Formation (P_2l_1) and the second member of the Lucaogou Formation (P_2l_2). Four sub-members are further divided, which are $P_2l_2^1$, $P_2l_2^2$, $P_2l_1^1$, and $P_2l_1^2$, respectively (Figure 2).

$P_2l_2^1$ is mainly composed of gray dolomitic mudstones with a small distribution area and a thin thickness (10–25 m), while $P_2l_2^2$ primarily consists of gray dolomitic sandstones, sandy dolarenite, and dolomitic mudstones. There is a tight reservoir interval in the $P_2l_2^2$, which is referred to as the upper reservoir interval (namely, the upper sweet spot), and it is speculated to be formed in the shallow lakes, with dominant beach and shoal carbonate deposits (average thickness of 50–140 m). $P_2l_1^1$ is mainly comprised of gray dolomitic mudstones, with a large distribution area and a huge average thickness (40–120 m). In comparison, $P_2l_1^2$ dominantly

TABLE 1 Fluid inclusions from calcite fillings from the Lucaogou Formation, Jimsar Sag, Junggar Basin.

Sample	Well	Depth (m)	Size (μm)	Quantity	Homogenization temperature ($^{\circ}\text{C}$)			Freezing temperature
					Minimum	Maximum	Average	
TF-1	J30	4,012.3	4	13	65.8	75.7	70.5	-3.3
TF-2	J30	4,015.2	5.7	6	76.2	86.7	80.8	-7.7
TF-3	J30	4,033.2	3	11	101.4	116.3	109.7	-5.5
TF-4	J30	4,035.6	6.6	15	180.9	196.7	189.4	-4.4
TF-5	J30	4,082.3	3	11	170.1	181.2	176.9	-5.5
TF-6	J30	4,085.6	4.4	7	49.1	61.8	53.2	-5.5
TF-7	J30	4,086.2	3.3	16	169.3	185.7	177.3	-6
TF-8	J30	4,121.5	5.4	15	185.3	197.8	189.9	-3.6
TF-9	J30	4,122.6	3.3	6	175.4	186.6	181.9	-6.3
TF-10	J30	4,123.4	4.5	7	102.7	113.0	106.7	-6.3
TF-11	J30	4,124.6	5.5	16	178.1	191.9	185.1	-2.7
TF-12	J30	4,152.8	4	15	79.5	95.8	87.0	-4.5
TF-13	J30	4,153.9	7.7	12	91.8	101.8	96.3	-5.4
TF-14	J30	4,196.8	4.8	15	136.2	149.1	141.9	-3.6
TF-15	J30	4,197.5	6.3	10	172.9	187.0	179.1	-2.7
TF-16	J30	4,199.4	4.8	5	69.6	82.4	75.7	-6.3
TF-17	J30	4,201.6	4.4	4	41.0	56.5	47.9	-6.3
TF-18	J30	4,235.6	4.4	16	75.6	88.0	80.5	-3.6
TF-19	J30	4,236.7	4.8	5	87.7	100.6	93.0	-7.2
TF-20	J30	4,237.2	4.4	13	95.0	108.4	102.4	-5.4
TF-21	J30	4,265.4	5	14	79.5	92.2	85.5	-6.3
TF-22	J30	4,266.8	4.8	10	78.3	93.5	85.9	-6.3
TF-23	J32	3,530.5	5.4	14	95.3	109.1	104.1	-4.5
TF-24	J32	3,531.4	2.4	12	133.7	145.9	138.9	-5.4
TF-25	J32	3,533.9	6.3	5	126.4	139.2	130.4	-7.2
TF-26	J32	3,570.5	6.6	13	177.1	187.1	182.9	-2.7
TF-27	J32	3,571.5	2.7	4	80.2	90.9	85.7	-4.5
TF-28	J32	3,572.6	6.6	5	86.1	96.0	91.5	-2.7
TF-29	J32	3,621.5	7	10	67.3	83.6	76.1	-7.2
TF-30	J32	3,625.4	6.3	5	161.4	172.6	167.9	-6.3
TF-31	J32	3,628.1	4	5	182.1	198.9	190.1	-2.7

(Continued on the following page)

TABLE 1 (Continued) Fluid inclusions from calcite fillings from the Lucaogou Formation, Jimsar Sag, Junggar Basin.

Sample	Well	Depth (m)	Size (μm)	Quantity	Homogenization temperature ($^{\circ}\text{C}$)			Freezing temperature
					Minimum	Maximum	Average	
TF-32	J32	3,645.9	6.3	8	94.3	107.2	102.7	-3.6
TF-33	J32	3,648.1	5.6	16	107.8	122.5	115.0	-3.6
TF-34	J32	3,649.7	4	11	129.3	139.3	134.8	-6.3
TF-35	J32	3,681.5	6	14	126.7	138.1	132.4	-7.2
TF-36	J32	3,687.6	4.4	14	131.5	145.5	136.6	-5.4
TF-37	J32	3,689.5	4.5	7	33.2	48.7	42.5	-7.2
TF-38	J32	3,751.4	7	10	84.4	100.5	93.2	-4.5
TF-39	J32	3,756.9	4.5	13	123.6	136.5	128.7	-3.6
TF-40	J32	3,758.5	3.6	5	143.0	158.2	149.7	-7.2
TF-41	J32	3,787.3	3.3	4	178.8	193.2	186.1	-7.2
TF-42	J32	3,788.6	4.5	5	196.7	209.9	202.7	-6.3
TF-43	J32	3,789.4	3.6	6	89.8	102.9	97.1	-2.7
TF-44	J174	3,126.4	3	9	132.6	147.4	140.6	-6.3
TF-45	J174	3,127.9	5.5	15	145.1	158.8	151.8	-5.4
TF-46	J174	3,128.5	3.3	13	116.4	128.0	123.5	-5.4
TF-47	J174	3,152.6	4.5	4	84.3	97.5	90.6	-6.3
TF-48	J174	3,153.4	6.3	7	168.7	179.4	174.4	-5.4
TF-49	J174	3,154.8	5.4	12	171.8	180.5	176.4	-6.3
TF-50	J174	3,227.6	4	5	133.1	149.7	141.8	-7.2
TF-51	J174	3,228.4	3	9	159.1	169.0	163.6	-4.5
TF-52	J174	3,229.1	2.4	15	120.0	131.5	126.8	-5.6
TF-53	J174	3,264.3	4.8	9	168.6	182.8	176.9	-4.8
TF-54	J174	3,265.1	4	14	168.4	185.8	177.1	-2.4
TF-55	J174	3,266.9	3.2	11	139.0	151.1	144.7	-3.2
TF-56	J174	3,294.6	5.5	4	170.6	180.5	176.3	-4
TF-57	J174	3,295.8	4.8	11	79.4	93.3	84.6	-4
TF-58	J174	3,296.4	6.3	15	84.6	97.4	92.1	-3.2
TF-59	J174	3,332.4	5.6	15	119.5	132.3	127.6	-6.4
TF-60	J174	3,334.8	3.3	4	133.4	146.6	139.3	-4.8
TF-61	J174	3,336.8	3.2	14	71.8	86.3	78.3	-5.6
TF-62	J015	2,156.1	2.4	12	140.8	150.2	145.4	-6.6

(Continued on the following page)

TABLE 1 (Continued) Fluid inclusions from calcite fillings from the Lucaogou Formation, Jimsar Sag, Junggar Basin.

Sample	Well	Depth (m)	Size (μm)	Quantity	Homogenization temperature ($^{\circ}\text{C}$)			Freezing temperature
					Minimum	Maximum	Average	
TF-63	J015	2,157.5	6	13	137.4	154.7	145.8	-7.7
TF-64	J015	2,261.3	5.4	7	77.4	93.1	84.2	-7.7
TF-65	J015	2,262.4	4	7	129.9	143.2	138.2	-7.7
TF-66	J015	2,263.8	2.7	13	187.5	201.2	193.4	-6.4
TF-67	J015	2,264.7	5	12	166.1	180.0	172.3	-4.8
TF-68	J015	2,330.6	5.4	15	189.5	202.0	194.8	-2.4
TF-69	J015	2,334.5	5.5	8	121.0	133.0	128.0	-3.2
TF-70	J015	2,335.9	4.4	8	205.7	218.0	210.3	-2.4
TF-71	J015	2,384.6	6	5	57.0	71.0	65.1	-4.8
TF-72	J015	2,385.1	3.2	14	133.7	144.1	138.2	-4.8
TF-73	J015	2,386.9	5	16	177.1	187.3	181.4	-4.8
TF-74	J015	2,387.5	4.4	4	88.4	101.3	93.3	-5.6
TF-75	J5	3,485.1	4	9	90.6	107.4	98.7	-4
TF-76	J5	3,486.6	3.2	5	135.5	149.3	142.4	-7.7
TF-77	J5	3,487.2	3	5	36.4	51.4	45.1	-7.7
TF-78	J5	3,488.6	3	14	84.6	96.8	90.9	-7.7
TF-79	J5	3,489.2	3.6	14	154.9	168.4	160.2	-6.6
TF-80	J5	3,502.6	2.4	11	194.4	208.9	200.1	-6.6
TF-81	J5	3,503.8	3.2	5	76.1	87.6	82.4	-4.4
TF-82	J5	3,504.1	2.7	16	96.1	107.0	100.1	-8.8
TF-83	J5	3,505.1	5.6	14	130.4	145.9	138.4	-5.5
TF-84	J5	3,542.6	5.5	9	58.0	71.3	64.7	-3.3
TF-85	J5	3,543.8	4.8	13	130.2	142.7	138.6	-6.6
TF-86	J5	3,544.1	2.7	8	90.4	101.9	95.2	-8.8
TF-87	J5	3,584.5	4	13	139.2	147.8	143.6	-6.4
TF-88	J5	3,585.7	6.3	16	189.1	202.3	193.5	-3.2
TF-89	J5	3,586.9	4.4	4	180.0	194.0	188.6	-2.4
TF-90	J5	3,587.1	3.3	13	177.5	191.9	186.4	-5.6
TF-91	J5	3,601.2	3.6	6	128.1	142.7	135.8	-3.2
TF-92	J5	3,602.3	3	16	165.8	176.3	171.5	-5.6

(Continued on the following page)

TABLE 1 (Continued) Fluid inclusions from calcite fillings from the Lucaogou Formation, Jimsar Sag, Junggar Basin.

Sample	Well	Depth (m)	Size (μm)	Quantity	Homogenization temperature ($^{\circ}\text{C}$)			Freezing temperature
					Minimum	Maximum	Average	
TF-93	J5	3,603.3	5.5	8	198.8	214.2	207.4	-2.4
TF-94	J5	3,604.8	6.3	9	93.3	108.8	100.0	-5.6
TF-95	J5	3,605.9	2.4	5	125.9	142.5	133.6	-5.6
TF-96	J251	3,560.4	4.8	6	78.5	90.5	83.5	-4.8
TF-97	J251	3,561.6	5	12	125.4	136.5	129.4	-5.6
TF-98	J251	3,562.8	6	10	180.1	192.8	188.4	-4
TF-99	J251	3,563.3	5.6	15	78.5	94.5	87.5	-5.6
TF-100	J251	3,564.1	3.6	13	136.7	152.3	143.6	-5.6
TF-101	J251	3,605.2	5.6	16	158.0	169.3	165.2	-3.2
TF-102	J251	3,606.7	3.2	9	79.5	92.5	87.9	-6.4
TF-103	J251	3,607.8	6	13	206.6	217.9	211.0	-2.4
TF-104	J251	3,608.2	6	16	79.9	90.7	86.7	-3.2
TF-105	J251	3,609.8	5	13	126.5	143.7	134.9	-2.4
TF-106	J251	3,612.5	3.3	6	139.4	151.4	143.7	-4.8
TF-107	J251	3,613.5	3.6	7	137.3	151.2	145.4	-4.8
TF-108	J251	3,614.9	6.3	8	159.7	170.9	165.5	-8.8
TF-109	J251	3,615.2	4.8	14	184.2	196.9	191.4	-4.4
TF-110	J251	3,664.3	3.3	14	73.3	87.3	80.3	-3.3
TF-111	J251	3,664.8	4.5	14	90.1	105.8	98.6	-6.6
TF-112	J251	3,665.1	4.5	9	83.5	94.2	89.9	-5.5
TF-113	J251	3,666.7	5	16	159.0	171.7	166.6	-7.7
TF-114	J251	3,667.2	5	11	161.0	174.6	168.6	-5.5
TF-115	J251	3,675.5	5.6	10	127.0	143.8	134.9	-8.8
TF-116	J251	3,675.9	6.6	16	137.5	149.7	141.9	-5.5
TF-117	J251	3,676.2	7	4	80.4	97.0	89.3	-6.6
TF-118	J251	3,677.8	6.6	5	108.9	121.1	114.7	-4.4
TF-119	J251	3,678.1	4	13	124.8	140.3	132.4	-8.8
TF-120	J251	3,724.3	7.7	12	165.8	176.5	172.4	-4.4
TF-121	J251	3,725.1	3.3	15	180.3	189.7	185.0	-5.5
TF-122	J251	3,726.9	4	9	180.4	197.1	188.9	-6.6
TF-123	J251	3,727.4	4	5	74.5	87.4	80.0	-6.6

(Continued on the following page)

TABLE 1 (Continued) Fluid inclusions from calcite fillings from the Lucaogou Formation, Jimsar Sag, Junggar Basin.

Sample	Well	Depth (m)	Size (μm)	Quantity	Homogenization temperature ($^{\circ}\text{C}$)			Freezing temperature
					Minimum	Maximum	Average	
TF-124	J251	3,751.3	5.4	4	164.2	177.8	170.1	-8.8
TF-125	J251	3,752.5	4.4	8	179.9	188.1	184.1	-3.3
TF-126	J251	3,753.7	4.4	13	124.4	138.8	130.7	-7.7
TF-127	J251	3,754.2	4.4	13	159.9	171.6	164.0	-6.6
TF-128	J251	3,785.4	5.5	6	51.4	63.3	57.6	-4.4
TF-129	J251	3,786.9	3.3	10	140.9	152.3	145.1	-4
TF-130	J251	3,787.2	4.4	10	144.1	153.3	148.8	-3.2
TF-131	J251	3,788.6	5	11	110.8	126.6	119.0	-3.2
TF-132	J251	3,789.7	7.7	10	166.8	177.7	170.9	-2.4
TF-133	J251	3,802.6	5.5	6	41.7	56.3	48.1	-4.8
TF-134	J251	3,803.5	6	10	88.2	101.0	96.2	-3.2
TF-135	J251	3,804.7	4.4	8	96.0	110.1	104.1	-6.4
TF-136	J251	3,805.8	6	6	152.5	163.1	157.9	-3.6
TF-137	J251	3,806.7	3	12	144.5	154.6	149.3	-3.6
TF-138	J251	3,835.7	3	8	190.6	204.0	196.4	-5.4
TF-139	J251	3,836.5	3.2	10	169.7	183.4	178.4	-3.6
TF-140	J251	3,837.2	4	6	85.2	100.8	92.0	-5.4
TF-141	J251	3,838.4	6	8	89.5	105.0	96.2	-6.3
TF-142	J251	3,839.5	3.6	10	174.4	187.6	182.1	-6.3
TF-143	J251	3,921.4	5.6	16	84.1	97.8	91.6	-2.7
TF-144	J251	3,922.8	3	10	136.3	147.5	143.5	-2.7
TF-145	J251	3,923.4	3.2	13	152.1	164.5	158.2	-4.5
TF-146	J251	3,924.8	6.3	16	159.6	173.6	167.3	-7.2
TF-147	J15	2,278.5	6	5	177.2	188.0	183.3	-4
TF-148	J15	2,279.6	4	4	120.1	132.9	126.5	-4.8
TF-149	J15	2,304.2	3.2	14	163.4	177.8	169.0	-6.3
TF-150	J15	2,305.7	5.4	9	59.7	73.1	68.5	-5.4
TF-151	J15	2,306.8	6.6	4	50.8	67.6	58.9	-3.6
TF-152	J15	2,325.9	2.7	8	81.6	94.9	89.7	-2.7
TF-153	J15	2,326.1	7.7	7	128.6	144.2	136.4	-2.7
TF-154	J15	2,367.8	5	11	132.6	145.1	137.0	-4.8

(Continued on the following page)

TABLE 1 (Continued) Fluid inclusions from calcite fillings from the Lucaogou Formation, Jimsar Sag, Junggar Basin.

Sample	Well	Depth (m)	Size (μm)	Quantity	Homogenization temperature ($^{\circ}\text{C}$)			Freezing temperature
					Minimum	Maximum	Average	
TF-155	J15	2,368.4	7	10	173.7	184.4	178.6	-4.8
TF-156	J15	2,369.1	5.5	7	155.7	169.0	163.0	-2.4
TF-157	J15	2,382.1	5.5	5	123.3	138.6	131.5	-5.6
TF-158	J15	2,383.6	5.4	11	128.6	142.0	135.1	-2.4
TF-159	J15	2,384.7	7.7	15	73.4	84.6	78.4	-7.7
TF-160	J15	2,385.9	4	9	98.5	112.4	107.1	-8.8

consists of gray dolomitic sandstones and dolomitic mudstones. There is another tight reservoir interval in the $P_2I_1^2$, which is referred to as the lower reservoir interval (namely, the lower sweet spot), and it is speculated to be formed in the deltaic front and shallow lakes, with dominant microfacies of delta front distal bar, sheet sand and shallow lacustrine deposits (average thickness of 30–60 m). Four small layers (STD-1~STD-4) are further classified in the upper sweet spot, while six small layers (XTD-1~XTD-6) are divided among the lower sweet spot, all of which are important tight reservoir intervals in the Jimsar Sag.

Natural fractures are developed in the Lucaogou Formation due to the strong tectonic activity, and they act as important reservoirs and seepage channels for fluids. As one of the important sources of fluids, deep magmatism-related hydrothermal fluids generally refer to the hydrothermal solutions released from magma during crystallization, which have strong migration ability and usually occur in the forms of fracture fillings.

3 Methods

3.1 Fluid inclusions

Fluid inclusion experiments were conducted in Research Institute of Petroleum Exploration Development. Linkam THMSG600 heating-freezing stage was prepared under a petrographic microscope and used for microscopic temperature measurement of fluid inclusions. The temperature measurement error was $\pm 0.2^{\circ}\text{C}$ at below 50°C and $\pm 2^{\circ}\text{C}$ at above 100°C . The freezing temperature and inclusion homogenization temperature were measured at a heating rate of $0.1^{\circ}\text{C}/\text{min}$. Salinity of the $\text{NaCl-H}_2\text{O}$ inclusion was calculated according to the freezing temperature of two-phase inclusions. The composition of the selected fluid inclusions was identified using an RM-2000 laser Raman microprobe containing an argon ion laser with a 514 nm laser source. The spectral scanning range was $100\text{--}4,300\text{ cm}^{-1}$, the accumulation time of each scan was 60 s, and the spectral resolution was $\sim 0.14\text{ cm}^{-1}$. After temperature measurement, the fluid inclusions were observed under a back scattering electron

microscope (BSEM) and scanning electron microscopy-cathode luminescence (SEM-CL). The BSEM and SEM-CL images of crack cement inclusions were recorded by a Quanta FEG 650 SEM device equipped with an energy dispersion spectrometer in Peking University. The accelerating voltage was 15 kV, and scanning time was 45 s.

3.2 C-O isotopes

C-O isotopes were tested on a Thermo-Finnigan MAT 253 isotope mass spectrometer in Guangzhou Institute of Geochemistry, Chinese Academy of Sciences. At each time, a sample (about 0.1 mg) was placed into a single reaction vessel and reacted with $1.92\text{ g}/\text{cm}^3\text{ H}_3\text{PO}_4$ at $90^{\circ}\text{C} \pm 1^{\circ}\text{C}$. Then the generated CO_2 was collected, purified, and transferred to a mass spectrometer. The international carbonate standard sample NBS-19 and the China national standard sample GBW04405 were repeatedly measured for comparison. The precision of $\delta^{13}\text{C}$ and $\delta^{18}\text{O}$ was $\pm 0.06\text{‰}(1\sigma)$ and $\pm 0.08\text{‰}(1\sigma)$ respectively.

3.3 Sm-Nd isochron age

As for Sm-Nd isotopic dating, pure calcite was manually sorted under binocular microscopy, and crushed in an agate mortar to 200 meshes. The isolated calcite was sent to detection of rare earth element (REE) concentrations on an ELAN 6000 inductively-coupled plasma mass spectrometer (ICP-MS) in Guangzhou Institute of Geochemistry, CAS. The Sm and Nd concentrations and isotope composition of the calcite were analyzed. Specifically, each sample was dissolved in a mixture of HF and perchloric acid (10: 1) in a polytetrafluoroethylene container (PTFE vessel), which was maintained below 150°C for at least 12 h until the whole sample was decomposed. Two portions of the same sample (each about 150 mg) were dissolved separately, and one portion was used for Sm and Nd concentration spiking and measurement, and the other was for detection of $^{143}\text{Nd}/^{144}\text{Nd}$ ratio. When Sm and Nd were separated through reversed phase extraction,

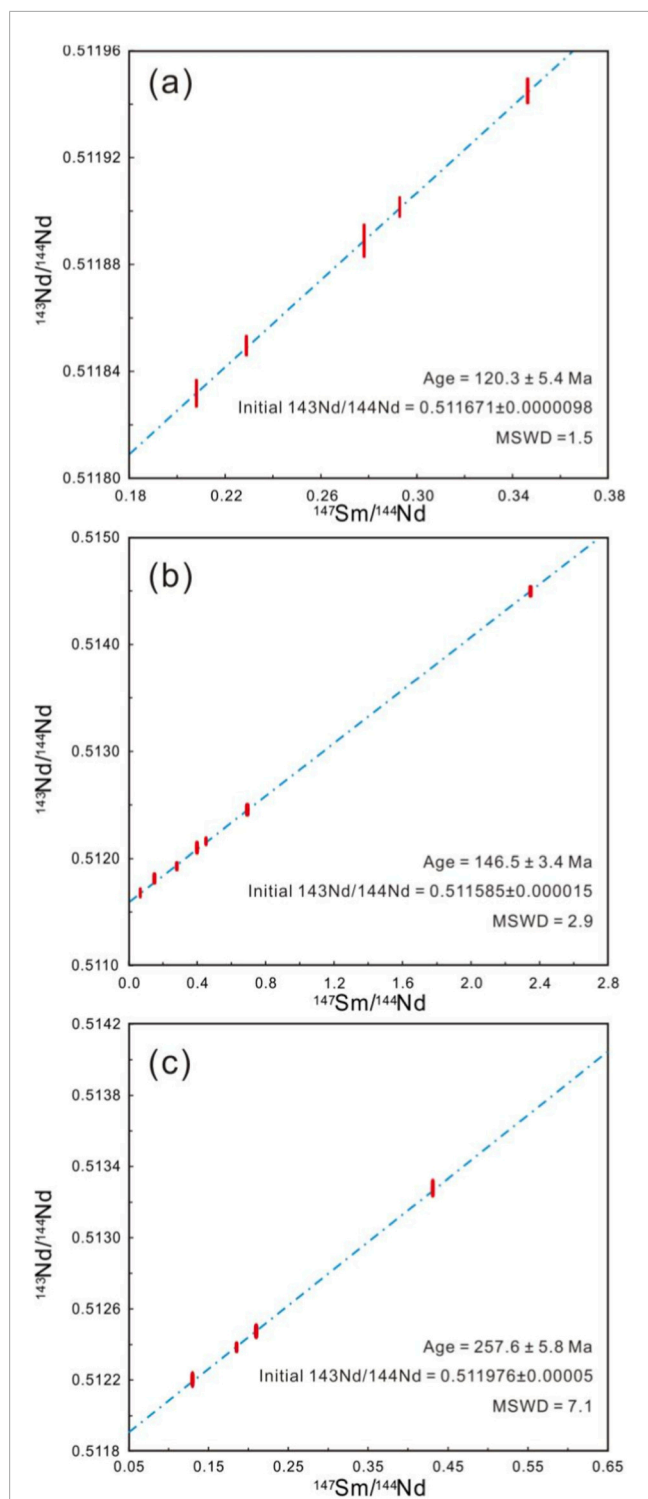


FIGURE 6
Sm-Nd isochrons for calcite cements in the tectonic fractures of the Lucaogou Formation in the Jimsar Sag, Junggar Basin. **(a)** The Sm-Nd isochron age of NW tensile fractures. **(b)** The Sm-Nd isochron age of NEE shear fracture. **(c)** The Sm-Nd isochron age of NNW shear fracture.

one key step was to coat di (6-methylheptyl) phosphate on polytetrafluoroethylene powder. The isotope ratio was measured on an IsoProbe T thermoionization mass spectrograph in Tianjin Geology Survey Center. The Nd ratio was normalized to the $^{146}\text{Nd}/^{144}\text{Nd}$ ratio, which was about 0.7219. The reproducibility of isotope ratio measurement was higher than 0.005% (2σ), and the precision of Sm and Nd concentration detection was smaller than the cited value of 0.5% (2σ). Experimental measurements showed the BCR-1 concentrations of Sm and Nd were 6.57 and 28.75 ppm respectively, and the $^{143}\text{Nd}/^{144}\text{Nd}$ ratio was 0.512644 ± 5 (2σ , $n = 6$). Repetitive analysis with the Johnson and Matthey[®] standard sample (JMC) showed the $^{143}\text{Nd}/^{144}\text{Nd}$ ratio was 0.511132 ± 5 (2σ , $n = 6$). The blank sample weights of Sm and Nd were 0.03 and 0.05 ng respectively. The attenuation constant ($\lambda^{147}\text{Sm}$) for age calculation was $6.54 \times 10^{-12}/\text{year}$. The Sm-Nd isochron ages were computed on ISOPLOT 2.9.

3.4 Nd isotope

As for Nd isotope, the powder samples were first labeled using a mixed isotopic tracer, then dissolved in HF and HNO_3 , and finally Nd and REEs were isolated. Isotopes were detected on a thermal ionization mass spectrogram in Tianjin Geology Survey Center. After measurements and according to BCR-1 and La Jolla Nd isotopic standards, the $^{143}\text{Nd}/^{144}\text{Nd}$ ratios were 0.512663 ± 9 (2σ) and 0.511862 ± 7 (2σ) respectively.

3.5 REEs

REEs were analyzed by ICP-MS, which can be used to detect sample solutions digested by HF + HClO_4 in closed containers. Quality control was ensured by using GBPG-1 and GSR-1. The relative standard deviations of trace element concentrations (including REEs) were smaller than 10%. The sample preparation, instrumental operation and calibration procedure proposed by Qi and Grégoire (2000) were adopted. The testing results of REEs were listed in appendix C, in which no valid results were obtained from samples TF-72 and TF-157 in group B and sample TF-101 from group C.

3.6 Acoustic emission of rocks

Totally 11 rock cores at different depths were selected from wells J32, J36, J174 and J176 for acoustic emission experiments. Uniaxial loading was induced by an RMT-159C rock mechanical testing system developed by Institute of Rock and Soil Mechanics, CAS, and acoustic emission was tested on the SAEU2S full-waveform track acoustic emission detector. This detector can acquire and record the value of acoustic emission, energy, number of rings, rise time, and usable voltage, and automatically generate

TABLE 2 Sm-Nd isochrons for calcite from the Lucaogou Formation, Jimsar Sag, Junggar Basin.

	w (Sm)/10 ⁻⁶	w (Nd)/10 ⁻⁶	¹⁴⁷ Sm/ ¹⁴⁴ Nd	1SE/*10 ⁻⁶	¹⁴³ Nd/ ¹⁴⁴ Nd	1SE/*10 ⁻⁶	Age
A Group	0.323	2.799	0.069486	0.000015	0.511672	0.000015	189.5Ma
A Group	0.363	0.799	0.283521	0.000016	0.511918	0.000016	189.6Ma
A Group	0.588	0.882	0.401485	0.000016	0.512075	0.000016	189.7Ma
A Group	0.584	0.777	0.452647	0.000012	0.512147	0.000012	189.8Ma
A Group	0.45	0.453	0.598273	0.000022	0.512326	0.000022	189.9Ma
A Group	0.749	0.295	1.529542	0.000016	0.513482	0.000016	189.10Ma
A Group	0.715	0.192	2.243877	0.000019	0.514369	0.000019	189.11Ma
A Group	0.227	0.9	0.151885	0.000017	0.511794	0.000017	189.12Ma
B Group	1.606	4.818	0.209166	0.000006	0.511833	0.000006	124.3Ma
B Group	2.512	6.113	0.257934	0.000008	0.511872	0.000008	124.4Ma
B Group	2.284	6.263	0.228847	0.000004	0.511848	0.000004	124.5Ma
B Group	4.075	7.588	0.337093	0.000005	0.511936	0.000005	124.6Ma
B Group	2.867	6.504	0.276649	0.000004	0.511889	0.000004	124.7Ma
C Group	5.02	12.7	0.2395	0.000007	0.512341	0.000007	272.4Ma
C Group	0.176	0.664	0.1601	0.000004	0.512184	0.000004	272.5Ma
C Group	0.397	0.238	1.0088	0.00001	0.513702	0.00001	272.6Ma
C Group	0.395	0.238	1.0064	0.00001	0.513701	0.00001	272.7Ma

interparameter relationship charts. All tests were conducted using an SR150Msyntony acoustic emission probe, and its displacement loading rate was 2×10^{-3} mm/s, center frequency was 60–400 kHz, sampling frequency was 5,000 Hz, parameter interval was 50, filter frequency was 20–100 kHz, waveform threshold was 40 dB, and gain of preamplifier loaded on two sides of a sample was 40 dB. Tests were started only when the parameters of the acoustic emission system were correctly calibrated. Each test was conducted after two repeated loadings. The sample was continually reloaded until it was completely destroyed.

4 Results and discussion

4.1 Fluid activity episodes

It is critical to characterize chemistry of fracture fillings in order to determine fluid activity episodes and corresponding paleoenvironments (Kerrick et al., 1984). When fluids enter fractures induced by tectonic stresses, a certain amount of crystalline minerals will precipitate and deposit on the fracture wall (Wendler et al., 2012; Griffiths et al., 2016).

Therefore, analysis of rock fracture history can promote effective identification of fluid activity episodes. In addition, geochemical and isotopic characteristics of fracture fillings in the core can further constrain division accuracy of fluid activity episodes.

Using the imaging logging data, we first obtain strike and inclination information of fractures in each well, and then plot corresponding rose diagrams showing the strikes of plane tectonic fractures (Figure 3a) and those of all the fractures (Figure 3b). There are mainly three sets of fractures in the study area, with NEE (45°–63°), NNW (317°–345°) and near NS (0°–27°) strikes, respectively (Figure 3c). Their distributions conform to certain rules. Specifically, the NEE fractures are mainly in the central and southern parts, the near NS ones are primarily in the northern and eastern parts, and the NNW ones are extensively distributed throughout the sag, though they are of low degree of development. According to their morphologies and crosscutting relationships, near NS fractures predate NEE ones, which further predate NNW ones. Dominant dip direction are in the range of 270°–360°.

When subjected to paleo-tectonic stress, corresponding memory will be recorded in the tight, brittle rocks (Segreto et al.,

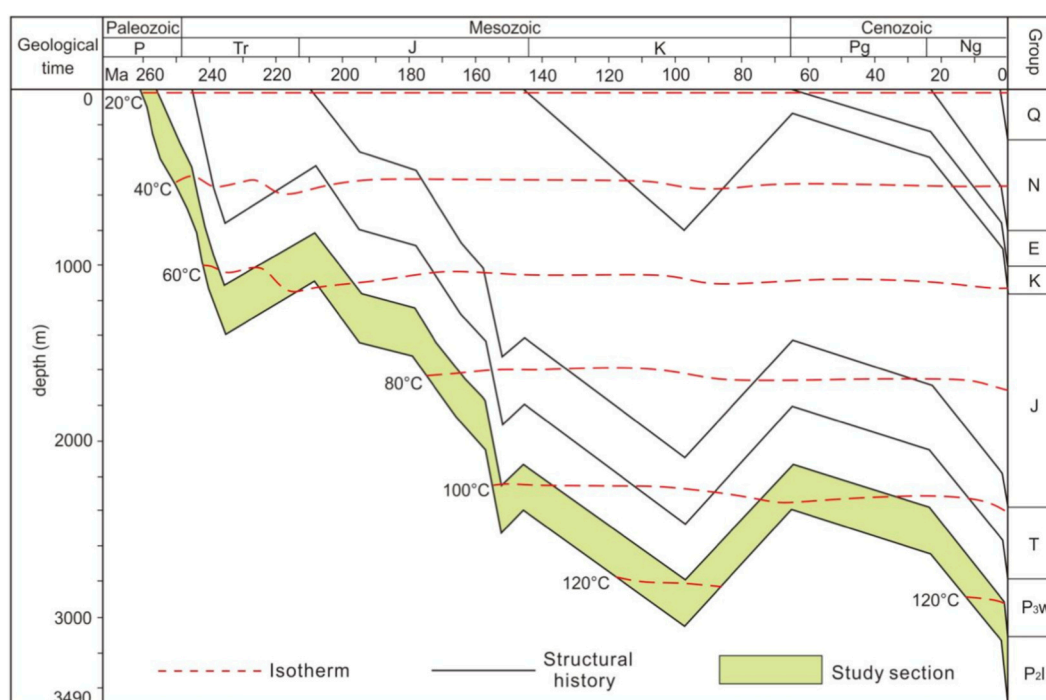


FIGURE 7
Burial history chart of the Lucaogou Formation in the Jimsar Sag, Junggar Basin.

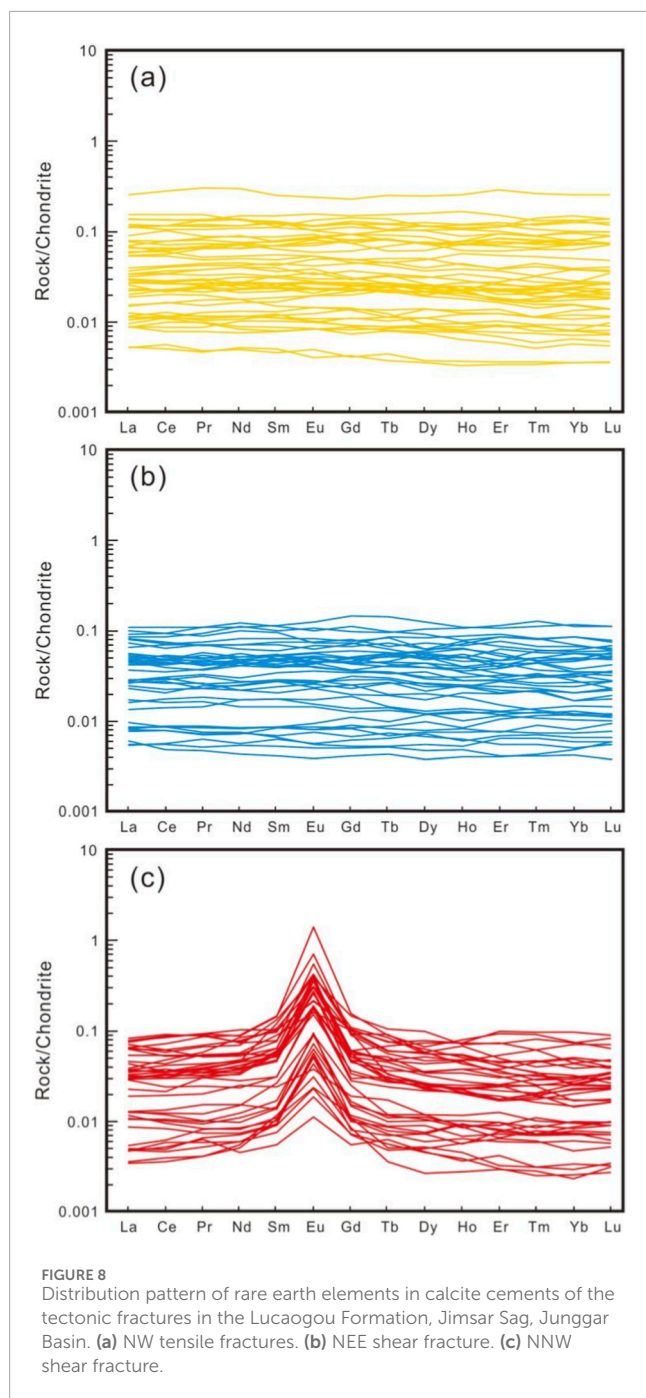
2015). In general, most of the underground rock formations are subjected to tectonic stress fields during Earth's history, accompanied by development of microscopic or concealed microfractures (Li et al., 2025; Luo et al., 2025). When the applied stress reaches the paleo-stress field strength, microfractures will begin to expand, resulting in sharply increasing quantity and intensity of acoustic emission. Accordingly, the stress applied at this point is supposed to be equivalent to the ancient stress field strength. Therefore, the number of Kaiser effect points appearing on the acoustic emission curve can be used to judge the minimum stress episodes and stress field strengths that the rock layer has experienced. Kaiser effect points in the acoustic emission curve correspond to those positions with stepwise sudden increases. However, the occurrence order of those steps does not necessarily indicate the sequential order of Kaiser effect points. All the other sub-figures in Figure 4 have four Kaiser effect points, which indicate at least four fracturing episodes. All the four Kaiser effect points in each sub-figure have a certain range of stress field strength variation, which demonstrates the corresponding fractures to be products of tectonic activities. However, we only observe three sets of fractures in the core, which might be attributable to the fact that two episodes of tectonic events result in the fractures with the same occurrence features.

Calcite fillings in the near NS tensile fractures have an average C-O isotope value of -5.43 and 10.23 , an average $\epsilon\text{Nd}(t)$ value of 8.79 and an average homogenization temperature of 165 – 195 °C. In comparison, those in the NEE shear fractures have an average C-O isotope value of -4.60 and 16.07 , an average $\epsilon\text{Nd}(t)$ value of

3.91 and an average homogenization temperature of 125 – 150 °C. What's more, those in the NNW shear fractures are featured by an average C-O isotope value of -0.93 and 21.12 , an average $\epsilon\text{Nd}(t)$ value of -2.14 and an average homogenization temperature of 75 – 105 °C (Figure 5; Table 1). Large differences in geochemical characteristics are seen among calcite fillings in three set of fractures, while homogeneity is observed within a certain set of fractures. Therefore, we suggest that there are mainly three independent episodes of fluid activities, given the distinct differences between the sets, no clear evidence for fluid mixing is observed. The Sm-Nd isochron ages of NW tensile fractures, NEE shear fracture and NNW shear fracture are 272.4 Ma, 189.5 Ma and 124.3 Ma, respectively (Figure 6; Table 2).

4.2 Fluid origin

Difference in fluid origins is speculated to be responsible for the difference in geochemical characteristics of calcite fillings. As shown in the burial history chart (Figure 7), the Permian Lucaogou Formation is at the deepest burial depth and has the highest burial temperature at this moment. Moreover, fluid inclusion homogenization temperatures of calcite fillings in near NS and NEE fractures are both higher than the current burial temperature, which implies a higher fluid temperature of the precipitated calcite than that of the surrounding rocks, and this is a typical feature of deep fluids (Machel and Lonnee, 2002; Davis and Smith, 2006).



In the high temperature environment, Eu^{3+} is reduced to Eu^{2+} , resulting in an increasing $\text{Eu}^{2+}/\text{Eu}^{3+}$ ratio, while an equilibrium is reached at 250 °C (Sverjensky, 1984; Bau and Möller, 1992; Cai et al., 2008; Zhu et al., 2013). Since the ionic radius of Eu^{2+} (0.117 nm) is larger than that of Eu^{3+} (0.095 nm), it is more difficult for Eu^{2+} to enter the rock-forming minerals than Eu^{3+} (Cai et al., 2008). Therefore, Eu^{2+} is the main form of Eu in the fluids at higher temperatures. Similarly, in the process of condensation and crystallization of hydrothermal fluids, Eu^{2+} is converted to Eu^{3+} , which further replace Ca^{2+} into carbonate

minerals due to its close ionic radius to that of Ca^{2+} (0.1 nm) (Zhu et al., 2013). In this case, the calcite fillings present a positive anomaly of Eu. This interpretation is based on the premise that the differentiation of Eu valence states is predominantly controlled by high-temperature reducing conditions. Although factors such as fluid–rock interaction may also influence the characteristics of the Eu anomaly, they do not alter the above assessment. Therefore, fluids corresponding to the calcite fillings in near NS and NEE fractures should be deep hydrothermal fluids according to their positive Eu anomalies (Figure 8; Table 3), which are in line with the high fluid inclusion homogenization temperatures.

As shown in Figure 9 and Table 4, calcite fillings in the near NS tensile fractures fall in the zone representing original mantle carbonates, which indicate relation of their origin to mantle fluids. In comparison, those in the NEE shear fractures present a transition from the original mantle carbonate zone to the sedimentary carbonate zone, reflecting the trend of fluid temperature reduction. Comparably, carbonates in the shear zone of the southern India show typical features of original mantle carbonates ($\delta^{18}\text{O}(\text{SMOW}) = 7.3\text{‰}$ to 8.5‰ , $\delta^{13}\text{C}(\text{PDB}) = -5.0\text{‰}$ to -4.7‰ ; Wichman et al., 1994). Meanwhile, calcite veins in the Dongying Sag, eastern China are speculated to be mantle fluids ($\delta^{18}\text{O}(\text{SMOW}) = 10.7\text{‰}$ to 13.1‰ , $\delta^{13}\text{C}(\text{PDB}) = -7.9\text{‰}$ to -7.3‰). Sharing similar C–O isotope features with above two examples, calcite fillings in the NEE shear fractures in the Jimsar Sag could also be related to mantle fluids. In addition, the narrow ranges of $\epsilon\text{Nd}(t)$ and C–O isotope values of the near NS tensile fractures and NEE shear fractures suggest small effects of assimilation of surrounding rocks and formation water.

Compared with calcite fillings in the NEE and NNW shear fractures, those in the near NS tensile fractures have the most depleted Nd isotopic compositions ($\epsilon\text{Nd}(t) = +6.44\sim+10.19$) (Figure 10). Moreover, recent studies suggest that the Junggar Basin and the surrounding Junggar Terrane share a common tectonic evolution from Carboniferous subduction–accretion process to Permian amalgamation, further confirming the relevant magmatism events in the north part of Xinjiang (Li et al., 2015). These magmatism events promote invasion of massive basalt magnesia–ultra-magnesium complexes in the upper crust. The Nd isotopic compositions of Permian mantle sources in the northern Xinjiang are represented by these Permian mafic rocks (Xiao et al., 2008; Gao and Zhou, 2013). These mantle sources can also account for the extremely depleted Nd isotopic compositions of the calcite fillings in the near NS tensile fractures in the Jimsar Sag based on the following evidence. (1) The Permian magnesia–ultra-magnesium complexes in the northern Xinjiang are generally featured by high $\epsilon\text{Nd}(t)$ values ranging from +6.2 to +8.5. (2) The $\epsilon\text{Nd}(t)$ values of mafic dykes of the Permian Beishan–Tianshan Region are +5.5 to +7.5 (Xue et al., 2016). (3) Olivine from the Tianshan massive unit also has high $\epsilon\text{Nd}(t)$ values, ranging from +6.0 to +7.5 (Gao and Zhou, 2013). (4) Basalts from the Junggar Basin have high $\epsilon\text{Nd}(t)$ values, ranging from $\sim+6.4$ to +8.0 (Li et al., 2015). All these suggest that the high $\epsilon\text{Nd}(t)$ values (from 6.44 to 10.19) of calcite fillings in the near NS tensile fractures are ascribed to thermal fluid activity induced by the mantle magmatism. This is further supported by the flatter partitioning of rare earth elements.

TABLE 3 Rare earth elements in calcite from the Lucaogou Formation, Jimsar Sag, Junggar Basin.

Group	Sample	La	Ce	Pr	Nd	Sm	Eu	Gd	Tb	Dy	Ho	Er	Tm	Yb	Lu
A Group	TF-2	0.00205	0.00598	0.00094	0.00413	0.00133	0.00049	0.0015	0.00029	0.00189	0.00036	0.00096	0.00013	0.00096	0.00014
A Group	TF-12	0.01805	0.04305	0.00687	0.03304	0.01205	0.00502	0.01888	0.00299	0.01852	0.00434	0.01529	0.00223	0.0133	0.00221
A Group	TF-13	0.007	0.01716	0.00272	0.01096	0.00364	0.00136	0.00449	0.00095	0.00587	0.00123	0.0029	0.00042	0.00297	0.00046
A Group	TF-16	0.05972	0.16841	0.02831	0.13697	0.03806	0.01363	0.04587	0.00927	0.06149	0.01422	0.04687	0.0066	0.04295	0.0064
A Group	TF-18	0.01858	0.0474	0.0075	0.03477	0.01168	0.00477	0.01869	0.00374	0.02582	0.00591	0.0184	0.00307	0.02198	0.00346
A Group	TF-19	0.00208	0.00478	0.00074	0.00354	0.00119	0.00048	0.00179	0.0003	0.00196	0.00043	0.00114	0.00015	0.00109	0.00015
A Group	TF-20	0.00227	0.00667	0.00103	0.00532	0.00183	0.00057	0.00188	0.00033	0.00209	0.00045	0.00127	0.00019	0.0012	0.00018
A Group	TF-21	0.00473	0.01353	0.00202	0.01057	0.00357	0.0012	0.00506	0.00101	0.0062	0.00152	0.00449	0.00081	0.00482	0.00068
A Group	TF-22	0.00359	0.00977	0.00164	0.00824	0.00225	0.00084	0.00275	0.00042	0.00279	0.00069	0.00203	0.00029	0.00224	0.00035
A Group	TF-23	0.00266	0.00693	0.00099	0.00495	0.00178	0.00071	0.0028	0.0005	0.00353	0.0007	0.00202	0.00028	0.00202	0.00029
A Group	TF-27	0.00674	0.01728	0.00279	0.01243	0.00373	0.00159	0.00549	0.00098	0.00551	0.00127	0.00356	0.00057	0.00403	0.00067
A Group	TF-28	0.01643	0.04688	0.00793	0.04121	0.0116	0.005	0.01635	0.00305	0.01815	0.00399	0.01379	0.00204	0.01316	0.00227
A Group	TF-29	0.02606	0.06342	0.00986	0.04976	0.01668	0.00597	0.02271	0.00388	0.02552	0.00498	0.01552	0.00227	0.01662	0.00246
A Group	TF-32	0.01357	0.03872	0.00641	0.0338	0.01045	0.00399	0.01599	0.00302	0.01878	0.00402	0.01126	0.00166	0.012	0.00187
A Group	TF-38	0.00639	0.01664	0.00237	0.01187	0.00349	0.00131	0.00455	0.00083	0.00543	0.00127	0.00282	0.00039	0.00265	0.00035
A Group	TF-43	0.02686	0.0694	0.01112	0.05361	0.01911	0.00587	0.01893	0.00339	0.02176	0.00408	0.01265	0.00183	0.01194	0.00187
A Group	TF-47	0.00545	0.0136	0.0023	0.01058	0.00402	0.00136	0.00477	0.00078	0.00539	0.00117	0.00302	0.00043	0.00334	0.00047
A Group	TF-57	0.00271	0.00771	0.00108	0.0054	0.00169	0.00063	0.00223	0.00041	0.00346	0.00075	0.00225	0.00029	0.00181	0.00028
A Group	TF-58	0.00792	0.02214	0.00354	0.0185	0.00543	0.00221	0.00629	0.00099	0.00642	0.00126	0.00375	0.00057	0.00404	0.00058
A Group	TF-61	0.02584	0.06971	0.0125	0.06915	0.02261	0.00892	0.03005	0.00571	0.03955	0.00935	0.02466	0.0033	0.02221	0.00294
A Group	TF-64	0.01261	0.03255	0.00454	0.02302	0.0074	0.00308	0.00929	0.00155	0.00921	0.00216	0.00602	0.00081	0.0064	0.00091
A Group	TF-74	0.03214	0.08042	0.01264	0.06379	0.01833	0.00651	0.02473	0.00444	0.02875	0.00653	0.01918	0.00267	0.01687	0.00249

(Continued on the following page)

TABLE 3 (Continued) Rare earth elements in calcite from the Lucaogou Formation, Jimsar Sag, Junggar Basin.

Group	Sample	La	Ce	Pr	Nd	Sm	Eu	Gd	Tb	Dy	Ho	Er	Tm	Yb	Lu
A Group	TF-75	0.00926	0.02535	0.00416	0.02067	0.0064	0.00284	0.01006	0.00166	0.0122	0.00319	0.00884	0.00132	0.00847	0.00121
A Group	TF-78	0.00265	0.00658	0.00092	0.00386	0.0012	0.00048	0.00166	0.00032	0.00224	0.00046	0.00149	0.00023	0.00134	0.00019
A Group	TF-81	0.00627	0.0167	0.00274	0.01452	0.00466	0.00162	0.00502	0.00092	0.00583	0.00138	0.0033	0.00052	0.0039	0.0005
A Group	TF-82	0.00642	0.01605	0.00251	0.0127	0.00405	0.0015	0.0051	0.00089	0.00499	0.00125	0.00356	0.00054	0.00385	0.00053
A Group	TF-86	0.00293	0.00701	0.00109	0.00534	0.00169	0.00059	0.00185	0.00033	0.00232	0.00049	0.00153	0.0002	0.00134	0.0002
A Group	TF-94	0.01407	0.03599	0.00491	0.02486	0.0084	0.00306	0.00985	0.00186	0.01265	0.00241	0.00636	0.00112	0.00655	0.00101
A Group	TF-96	0.00674	0.016	0.00248	0.01258	0.00486	0.0017	0.00606	0.00122	0.00666	0.00128	0.00438	0.0006	0.00445	0.00066
A Group	TF-99	0.00353	0.00992	0.00142	0.00764	0.00254	0.00111	0.00401	0.00084	0.00538	0.00109	0.00284	0.00045	0.00338	0.00051
A Group	TF-102	0.00747	0.0204	0.00307	0.01565	0.0048	0.002	0.00597	0.00119	0.00775	0.00189	0.00503	0.00069	0.00452	0.00086
A Group	TF-104	0.00122	0.00342	0.00045	0.0023	0.0007	0.00029	0.00083	0.00017	0.00095	0.00021	0.0006	0.00009	0.00061	0.00009
A Group	TF-110	0.03167	0.08146	0.01227	0.06202	0.01724	0.00766	0.02889	0.00505	0.02871	0.0061	0.01829	0.0035	0.02506	0.00343
A Group	TF-111	0.00209	0.00533	0.00082	0.00476	0.00155	0.00057	0.00225	0.00038	0.00278	0.00055	0.00167	0.00024	0.00158	0.00023
A Group	TF-112	0.01576	0.03681	0.00633	0.02987	0.01052	0.00424	0.01598	0.003	0.01848	0.00346	0.00993	0.00161	0.01053	0.00177
A Group	TF-117	0.01529	0.03995	0.00608	0.03037	0.01049	0.00459	0.01517	0.00225	0.01556	0.00406	0.01253	0.00188	0.01353	0.00187
A Group	TF-123	0.0025	0.00691	0.00119	0.00612	0.00196	0.00084	0.00289	0.00046	0.00238	0.00054	0.00146	0.00023	0.00136	0.00025
A Group	TF-134	0.00124	0.00305	0.00044	0.00242	0.00077	0.00023	0.00086	0.00014	0.0009	0.00019	0.00056	0.00009	0.0006	0.00009
A Group	TF-135	0.02781	0.07002	0.01065	0.05295	0.01874	0.00658	0.02499	0.00388	0.02894	0.0059	0.01651	0.00227	0.01602	0.00225
A Group	TF-140	0.03574	0.09274	0.01442	0.06127	0.01938	0.00666	0.02604	0.00445	0.03159	0.00668	0.02033	0.00294	0.02112	0.00315
A Group	TF-141	0.0052	0.01394	0.00233	0.01211	0.00407	0.00157	0.00525	0.00099	0.0059	0.00138	0.00377	0.00049	0.00316	0.00047
A Group	TF-143	0.008	0.02093	0.00354	0.01862	0.00598	0.00191	0.00741	0.00126	0.00797	0.00163	0.0042	0.00063	0.00461	0.00065
A Group	TF-152	0.00597	0.01306	0.00222	0.00982	0.0033	0.00133	0.00455	0.0008	0.00483	0.00101	0.0027	0.00036	0.00259	0.00035
A Group	TF-159	0.01274	0.03379	0.00606	0.0327	0.00961	0.00339	0.01239	0.00256	0.01929	0.00399	0.01186	0.00194	0.01255	0.00185
B Group	TF-14	0.00219	0.00514	0.00077	0.00372	0.00128	0.00048	0.00168	0.00032	0.00243	0.00046	0.00168	0.00029	0.00192	0.00027

(Continued on the following page)

TABLE 3 (Continued) Rare earth elements in calcite from the Lucaogou Formation, Jimsar Sag, Junggar Basin.

Group	Sample	La	Ce	Pr	Nd	Sm	Eu	Gd	Tb	Dy	Ho	Er	Tm	Yb	Lu
B Group	TF-24	0.0064	0.01831	0.00306	0.01374	0.00508	0.00201	0.0068	0.00128	0.00765	0.00169	0.00519	0.0008	0.0053	0.00069
B Group	TF-25	0.00971	0.0262	0.00405	0.0185	0.00724	0.00219	0.00722	0.00123	0.00868	0.00154	0.00464	0.00065	0.00444	0.00067
B Group	TF-34	0.01057	0.02349	0.00336	0.0188	0.00587	0.0024	0.01015	0.00204	0.01431	0.00346	0.00907	0.00113	0.00823	0.00118
B Group	TF-35	0.00667	0.01692	0.0029	0.01245	0.00412	0.00149	0.00628	0.00108	0.00635	0.00133	0.00446	0.00061	0.00396	0.00068
B Group	TF-36	0.00177	0.00469	0.00064	0.00326	0.00124	0.00045	0.00164	0.00025	0.00187	0.00042	0.00124	0.00018	0.00121	0.00019
B Group	TF-39	0.0151	0.04168	0.00643	0.02829	0.00885	0.00388	0.01343	0.00264	0.01542	0.00352	0.00853	0.00118	0.00801	0.00123
B Group	TF-40	0.00966	0.02502	0.00428	0.02	0.00604	0.00245	0.00735	0.0015	0.01095	0.00188	0.00488	0.00083	0.00459	0.00057
B Group	TF-44	0.01119	0.02898	0.00423	0.02089	0.00729	0.00258	0.00872	0.00164	0.01073	0.00223	0.00544	0.00076	0.00556	0.0008
B Group	TF-50	0.02536	0.06559	0.01005	0.04937	0.017	0.00706	0.02901	0.00522	0.031	0.00598	0.01716	0.00281	0.01921	0.00275
B Group	TF-52	0.00397	0.00947	0.00152	0.00655	0.00215	0.00081	0.00249	0.00047	0.00298	0.00055	0.00185	0.00027	0.00169	0.00025
B Group	TF-55	0.01093	0.03162	0.00468	0.02306	0.00804	0.00325	0.0119	0.00208	0.01271	0.0025	0.00748	0.00125	0.00929	0.00127
B Group	TF-59	0.00126	0.00326	0.00047	0.00246	0.00077	0.00028	0.001	0.00019	0.00115	0.00026	0.00067	0.0001	0.00069	0.00009
B Group	TF-60	0.00198	0.00514	0.00079	0.00377	0.00127	0.00053	0.0022	0.00036	0.00289	0.00067	0.00203	0.00031	0.00214	0.00029
B Group	TF-62	0.01092	0.02789	0.00499	0.02202	0.0078	0.00314	0.01006	0.00205	0.01473	0.00397	0.01394	0.00197	0.01413	0.00185
B Group	TF-63	0.02116	0.05642	0.00813	0.0451	0.01427	0.00417	0.01456	0.00228	0.0134	0.00276	0.01013	0.00142	0.00918	0.00135
B Group	TF-65	0.01015	0.02594	0.00392	0.01859	0.00701	0.00289	0.00851	0.00165	0.01375	0.00282	0.00689	0.0011	0.00576	0.00086
B Group	TF-69	0.00568	0.01344	0.00213	0.01005	0.00308	0.00129	0.00389	0.0007	0.00424	0.00113	0.00323	0.00055	0.0028	0.00047
B Group	TF-76	0.00845	0.02066	0.00345	0.01998	0.00601	0.00225	0.00722	0.00127	0.0072	0.00154	0.00452	0.00076	0.0051	0.00088
B Group	TF-83	0.01907	0.04499	0.00635	0.03168	0.01112	0.00424	0.01617	0.00242	0.0182	0.00381	0.01247	0.00168	0.01112	0.00159
B Group	TF-85	0.01683	0.03858	0.00642	0.03206	0.01036	0.00351	0.01419	0.00311	0.02088	0.00483	0.01485	0.00203	0.01165	0.00153
B Group	TF-87	0.00187	0.00518	0.00081	0.00384	0.00127	0.00045	0.00178	0.0003	0.00195	0.00045	0.0012	0.00022	0.00133	0.00023
B Group	TF-91	0.00184	0.00463	0.00066	0.0033	0.00102	0.00043	0.00135	0.00026	0.00164	0.00034	0.00088	0.00014	0.00084	0.00014

(Continued on the following page)

TABLE 3 (Continued) Rare earth elements in calcite from the Lucaogou Formation, Jimsar Sag, Junggar Basin.

Group	Sample	La	Ce	Pr	Nd	Sm	Eu	Gd	Tb	Dy	Ho	Er	Tm	Yb	Lu
B Group	TF-95	0.00604	0.01788	0.00239	0.01211	0.00428	0.0016	0.00498	0.00098	0.00534	0.00134	0.00352	0.00052	0.00276	0.00044
B Group	TF-97	0.00632	0.01558	0.00244	0.00997	0.00358	0.00145	0.0046	0.00095	0.00654	0.00138	0.00385	0.00057	0.00337	0.00057
B Group	TF-100	0.0187	0.04281	0.00698	0.03693	0.01212	0.0046	0.01541	0.00307	0.01563	0.00421	0.01073	0.00153	0.00966	0.00147
B Group	TF-101	0.00326	0.00889	0.00112	0.00564	0.00189	0.00085	0.00221	0.00033	0.00194	0.00047	0.00119	0.00018	0.00131	0.0002
B Group	TF-106	0.00525	0.01228	0.00225	0.01124	0.00406	0.00133	0.00501	0.00072	0.00493	0.00101	0.00242	0.00033	0.00198	0.0003
B Group	TF-107	0.01212	0.02822	0.00429	0.02308	0.00808	0.00255	0.0091	0.00204	0.01175	0.00281	0.0063	0.00108	0.00757	0.00129
B Group	TF-115	0.01268	0.02865	0.00534	0.02314	0.00773	0.00281	0.00858	0.00145	0.0097	0.00209	0.00655	0.00124	0.00801	0.00143
B Group	TF-116	0.00195	0.00508	0.00069	0.00344	0.00098	0.00031	0.00105	0.00019	0.00136	0.00029	0.00103	0.00016	0.00097	0.00015
B Group	TF-119	0.00123	0.00334	0.00058	0.00256	0.00092	0.00032	0.00124	0.00024	0.00177	0.00033	0.00111	0.00017	0.00108	0.00016
B Group	TF-126	0.01066	0.02671	0.00392	0.02197	0.00687	0.00255	0.00976	0.00187	0.01262	0.00222	0.00701	0.00092	0.00586	0.00085
B Group	TF-129	0.00366	0.01054	0.0017	0.00776	0.00263	0.00087	0.00275	0.00051	0.00297	0.0007	0.00188	0.00031	0.0019	0.00028
B Group	TF-130	0.00139	0.00288	0.00044	0.00194	0.00061	0.00021	0.00082	0.00016	0.00092	0.00022	0.00064	0.00011	0.0008	0.00014
B Group	TF-137	0.01157	0.02846	0.00381	0.02038	0.00632	0.00276	0.00882	0.00197	0.01251	0.00301	0.0076	0.0015	0.01009	0.00169
B Group	TF-144	0.00618	0.01619	0.00213	0.01137	0.00424	0.00152	0.00571	0.00105	0.00592	0.00132	0.0033	0.00055	0.00339	0.00054
B Group	TF-148	0.02327	0.05636	0.01009	0.05523	0.01665	0.00568	0.02253	0.00358	0.0227	0.00435	0.01373	0.00205	0.01431	0.00194
B Group	TF-153	0.01957	0.05079	0.00875	0.05045	0.01505	0.006	0.01965	0.00347	0.02585	0.00585	0.01858	0.00316	0.01864	0.0028
B Group	TF-154	0.00311	0.00842	0.00134	0.00772	0.00259	0.00097	0.00375	0.00052	0.00319	0.00076	0.00208	0.00034	0.00244	0.00036
B Group	TF-158	0.01306	0.03058	0.00455	0.0257	0.00734	0.00295	0.00979	0.00155	0.00967	0.00197	0.00611	0.00111	0.00617	0.00103
C Group	TF-4	0.01575	0.03568	0.00643	0.03278	0.02031	0.02215	0.03032	0.0039	0.02536	0.00407	0.01236	0.0016	0.0076	0.00124
C Group	TF-5	0.00777	0.01894	0.00336	0.01959	0.00812	0.01063	0.00996	0.00153	0.00826	0.0016	0.00431	0.00076	0.00538	0.00087
C Group	TF-7	0.0021	0.00525	0.00072	0.00355	0.00147	0.00297	0.00168	0.00027	0.00188	0.00033	0.00129	0.00018	0.00136	0.0002
C Group	TF-8	0.00088	0.00248	0.0004	0.00263	0.00183	0.00181	0.0018	0.00014	0.0007	0.00016	0.0005	0.00007	0.00041	0.00008
C Group	TF-9	0.00118	0.0029	0.0005	0.00285	0.00118	0.0011	0.00154	0.00022	0.00119	0.00022	0.00051	0.00007	0.00045	0.00007

(Continued on the following page)

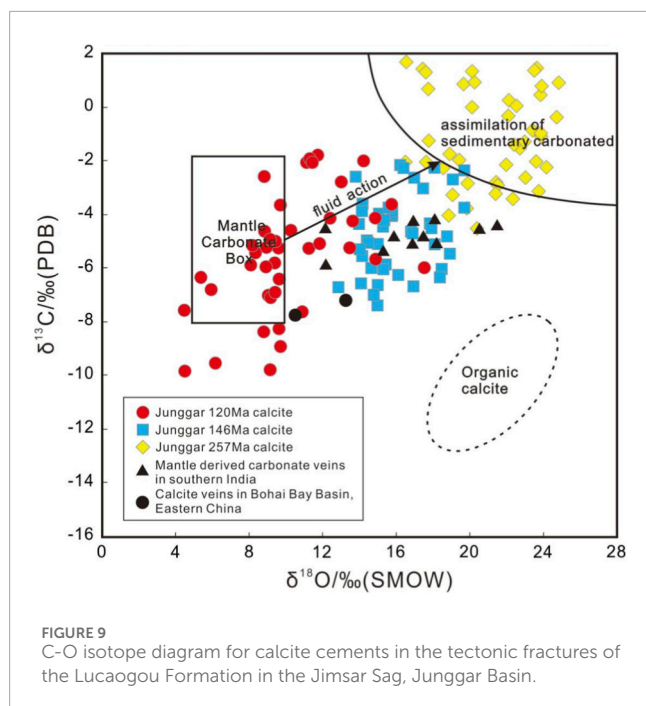
TABLE 3 (Continued) Rare earth elements in calcite from the Lucaogou Formation, Jimsar Sag, Junggar Basin.

Group	Sample	La	Ce	Pr	Nd	Sm	Eu	Gd	Tb	Dy	Ho	Er	Tm	Yb	Lu
C Group	TF-11	0.01801	0.05313	0.00888	0.0413	0.02187	0.08049	0.03191	0.00335	0.01696	0.00455	0.01548	0.00235	0.01275	0.00163
C Group	TF-15	0.00688	0.0148	0.00238	0.01119	0.00482	0.01007	0.00582	0.00092	0.00566	0.00121	0.00321	0.00042	0.00257	0.00042
C Group	TF-26	0.00459	0.01212	0.00193	0.01178	0.00371	0.00223	0.00399	0.00066	0.00307	0.00068	0.00212	0.00027	0.00167	0.00023
C Group	TF-30	0.00884	0.02552	0.00417	0.02183	0.01857	0.02424	0.01975	0.00124	0.00686	0.00131	0.00404	0.00064	0.00477	0.00087
C Group	TF-31	0.0055	0.01315	0.00295	0.01338	0.00484	0.01095	0.00616	0.00119	0.00581	0.00118	0.00293	0.00053	0.00381	0.00059
C Group	TF-41	0.01681	0.03836	0.005	0.02468	0.00992	0.02179	0.01248	0.00258	0.01894	0.00423	0.01628	0.00247	0.01644	0.00227
C Group	TF-48	0.00257	0.00653	0.00096	0.00582	0.00264	0.00526	0.00308	0.00038	0.00263	0.00059	0.00163	0.00019	0.0015	0.00026
C Group	TF-49	0.00308	0.00733	0.00099	0.00462	0.00216	0.00368	0.00323	0.00044	0.00275	0.00049	0.00165	0.00022	0.00173	0.00025
C Group	TF-53	0.00744	0.0198	0.0031	0.01559	0.00903	0.01497	0.01077	0.00127	0.00645	0.00132	0.00418	0.00049	0.00395	0.0006
C Group	TF-54	0.01505	0.03839	0.00661	0.03674	0.01542	0.01259	0.02144	0.00282	0.02004	0.00416	0.01197	0.0021	0.0125	0.00211
C Group	TF-56	0.00893	0.02153	0.00376	0.02112	0.00981	0.02284	0.01069	0.00171	0.00885	0.00197	0.00512	0.00085	0.00451	0.0008
C Group	TF-66	0.00115	0.00325	0.00062	0.00217	0.00086	0.00067	0.00117	0.00023	0.0012	0.00021	0.0007	0.000085	0.00052	0.00009
C Group	TF-67	0.00862	0.02196	0.00397	0.02264	0.0088	0.01775	0.01209	0.00178	0.01116	0.00261	0.00577	0.00081	0.00527	0.00075
C Group	TF-68	0.00822	0.02259	0.00447	0.02424	0.00843	0.01719	0.00972	0.00177	0.01224	0.00159	0.00468	0.0009	0.00535	0.00089
C Group	TF-73	0.00832	0.02347	0.00329	0.01653	0.00926	0.01041	0.01153	0.00113	0.00683	0.0012	0.00286	0.00049	0.00295	0.00044
C Group	TF-88	0.01547	0.04478	0.00827	0.04209	0.02256	0.04048	0.01908	0.00343	0.01478	0.00388	0.00832	0.00104	0.0075	0.00099
C Group	TF-89	0.00918	0.02944	0.00561	0.03991	0.01497	0.02371	0.0227	0.00317	0.01424	0.00305	0.00686	0.0009	0.00435	0.00063
C Group	TF-90	0.00121	0.00307	0.00064	0.00338	0.0014	0.00135	0.00149	0.00018	0.00129	0.00033	0.00109	0.00016	0.00083	0.00014
C Group	TF-92	0.00793	0.02159	0.00363	0.02114	0.00794	0.0088	0.00757	0.00107	0.00616	0.00136	0.0037	0.00053	0.00443	0.00064
C Group	TF-98	0.01092	0.02656	0.00525	0.02625	0.00835	0.02047	0.01132	0.00195	0.00897	0.00214	0.00633	0.00115	0.00838	0.00103
C Group	TF-108	0.01985	0.05654	0.00845	0.03544	0.01646	0.01778	0.0195	0.00224	0.01475	0.00247	0.00605	0.00075	0.00503	0.00089
C Group	TF-109	0.00715	0.02074	0.00305	0.01813	0.00741	0.02026	0.00963	0.00115	0.00672	0.00143	0.0043	0.00063	0.0029	0.00046
C Group	TF-113	0.01043	0.02185	0.00339	0.01752	0.00713	0.01586	0.00694	0.00102	0.00661	0.00127	0.00294	0.00052	0.00252	0.00042

(Continued on the following page)

TABLE 3 (Continued) Rare earth elements in calcite from the Lucaogou Formation, Jimsar Sag, Junggar Basin.

Group	Sample	La	Ce	Pr	Nd	Sm	Eu	Gd	Tb	Dy	Ho	Er	Tm	Yb	Lu
C Group	TF-114	0.01846	0.05173	0.00884	0.04854	0.01587	0.01225	0.02129	0.00287	0.01607	0.00288	0.00695	0.00088	0.00551	0.00069
C Group	TF-120	0.00114	0.00364	0.00057	0.00283	0.00143	0.00332	0.00218	0.00028	0.00156	0.00037	0.00101	0.00015	0.00106	0.00015
C Group	TF-121	0.01854	0.05423	0.00866	0.03431	0.01198	0.01734	0.01249	0.0018	0.01335	0.00269	0.00895	0.00159	0.01212	0.0018
C Group	TF-122	0.0031	0.00836	0.00149	0.00731	0.00214	0.00419	0.00344	0.00042	0.00288	0.00052	0.00151	0.00028	0.00165	0.00025
C Group	TF-124	0.00132	0.00392	0.00079	0.00406	0.00159	0.00252	0.00209	0.00033	0.00194	0.00054	0.00133	0.00023	0.00144	0.00024
C Group	TF-125	0.00261	0.0063	0.0009	0.00524	0.00224	0.00553	0.00231	0.0003	0.00187	0.00053	0.00137	0.00019	0.0013	0.00016
C Group	TF-132	0.00699	0.01842	0.00293	0.01599	0.00848	0.01105	0.0099	0.00108	0.00612	0.00115	0.00286	0.00046	0.00345	0.00059
C Group	TF-139	0.01515	0.03265	0.0051	0.026	0.01189	0.03172	0.01838	0.00213	0.01213	0.00272	0.00763	0.00119	0.00869	0.00119
C Group	TF-142	0.00084	0.00226	0.0004	0.00243	0.00165	0.00308	0.00228	0.00019	0.00134	0.00026	0.00056	0.00008	0.00059	0.00008
C Group	TF-146	0.00281	0.00594	0.00081	0.00389	0.00172	0.00139	0.00242	0.00034	0.00233	0.0004	0.00122	0.00018	0.00124	0.00019
C Group	TF-147	0.01281	0.03291	0.00518	0.02683	0.01377	0.00864	0.021	0.00228	0.01439	0.00312	0.00745	0.00121	0.00657	0.00104
C Group	TF-149	0.00305	0.00775	0.00117	0.00711	0.00414	0.00531	0.00516	0.00045	0.00308	0.0005	0.00112	0.00021	0.00128	0.00018
C Group	TF-155	0.00719	0.02016	0.00358	0.01845	0.00877	0.01587	0.00937	0.00138	0.00921	0.00218	0.00532	0.00065	0.00428	0.00078



Calcite fillings in the NEE shear fractures are characterized by moderate to high positive $\epsilon\text{Nd}(t)$ values, indicating significant contribution from mantle-like components. However, $\epsilon\text{Nd}(t)$ values of calcite fillings in the NEE shear fractures are slightly different from those in the near NS tensile fractures and mafic rocks in the northern Xinjiang, which indicates different fluid origins of calcite fillings in two sets of fractures. This is further demonstrated by the difference in the C-O isotope system (Figure 9). In terms of partitioning of rare earth elements, calcite fillings in the NEE shear fractures are characterized by light rare earth element enrichment, which is a typical feature of crustal fluids. Therefore, we infer that calcite fillings in the NEE shear fractures are juvenile crustal-derived in nature, but also present mantle-like isotopic characteristics. Calcite fillings in the NEE shear fractures share similar $\epsilon\text{Nd}(t)$ values (from -0.52 to 6.27) with granites in the northern Xinjiang, which are speculated to be mainly-derived from lower continent crust (Zhang et al., 2018). The basement beneath the Junggar Basin has been interpreted as a complex, from sedimentary unit to volcanic unit (Li et al., 2015), and basalts beneath the Junggar Basin are speculated to be generated by partial melting of the metasomatized wedge mantle by hydrous fluids and melts of subducted sediments. Therefore, the relatively low $\epsilon\text{Nd}(t)$ values of calcite fillings in the shear fractures are likely products of the lower crust magmatism, which means their origin is related to magmatism of mixed basalts and sedimentary basement.

As for calcite fillings in the NNW shear fractures, they fall in the zone representing sedimentary carbonates. In conjunction with the negative $\epsilon\text{Nd}(t)$ values and low fluid inclusion homogenization temperatures, we suggest them to originate from basin fluids in the Jimsar Sag.

4.3 Coupling of fluid activity and tectonic evolution history

As direct products of regional tectonic activity, tectonic fractures provide migration channel and reservoir space for deep fluids. As demonstrated in the acoustic emission curve (Figure 4), there are mainly four episodes of tectonic activities. Meanwhile, according to different fluid inclusion homogenization temperatures of calcite fillings in the three sets of fractures and homogeneous geochemical features within one set of fractures, we infer that there are mainly three episodes of tectonic-fluid filling events, accompanied by no occurrence of fluid mixing. Three sets of fractures are filled by fluids at 272.4, 189.5, and 124.3 Ma, respectively, based on analysis of Sm-Nd isochron ages, which are consistent with crosscutting relationships among them recognized in the field outcrops.

As an important part of the Central Asian Orogenic Belt, the northern Xinjiang is characterized by development of the Paleozoic orogenic belt that dominantly consists of continental crust accretion. During the Late Carboniferous, collision among continents of the Junggar Basin and folding orogenic movement become intensified, which result in development of fault basin and intracontinental rift, accompanied by widely distributed, frequently occurring magmatic and volcanic activities. Subsequently, the post-collision mantle-derived magmatism is extensively developed in the northern Xinjiang during the Permian, which marks the entrance of the Junggar Basin into the post-collision extensional period. At the same time, the emergence of the Santai Uplift in the Jimsar Sag leads to different episodes of tectonic stresses, associated with two episodes of fracturing events (Liu et al., 2019). According to the Sm-Nd isochron ages of calcite fillings, the Jimsar Sag is under a tensile tectonic setting before 272.4 Ma, after which NS extrusion generates a large amount of NS tensile fractures. Then, mantle magmatism-related fluids enter these tensile fractures, forming calcite fillings with high $\epsilon\text{Nd}(t)$ contents, high $\delta^{18}\text{O}$ values and high fluid inclusion homogenization temperatures. At 189.5 Ma, the compressive stress from the southwest to the northeast leads to formation of NEE shear fractures, and crustal magmatism-related fluids invade these fractures, forming calcite fillings with second highest $\epsilon\text{Nd}(t)$ contents, second highest $\delta^{18}\text{O}$ values and second highest fluid inclusion homogenization temperatures. During the Early Cretaceous, the Bogda Piedmont Foreland Depression experiences persistent foldbacks under the tectonic stress (Shen et al., 2006; Tang et al., 2015). Later at 124.3 Ma, the Fukang Fault Belt in the southern part of the Jimsar Sag becomes intensively active, exhibiting strong overthrust features from south to north. During this period, NNW shear fractures emerge and basin fluids enter these fractures, forming calcite fillings with low $\epsilon\text{Nd}(t)$, low $\delta^{18}\text{O}$ values and low fluid inclusion homogenization temperatures.

5 Conclusion

The geophysical, isotopic, geochemical, and geochronological data presented in this study are in good agreement with each other. They collectively support the argument that the Jimsar Sag experiences three episodes of fluid activities during corresponding

TABLE 4 Nd-C-O isotopic compositions of calcite from the Lucaogou Formation, Jimsar Sag, Junggar Basin.

Group	Sample	Age	2sm	$^{143}\text{Nd}/^{144}\text{Nd}$	2sm	Nd (ppm)	Sm (ppm)	$^{147}\text{Sm}/^{144}\text{Nd}$	$\epsilon\text{Nd}(t)$	$\delta^{18}\text{O}(\text{SMOW})$	$\delta^{13}\text{C}(\text{PDB})$	Age
A Group	TF-2	0.124	11	0.512596	5	4.8	2.21	0.278346	-2.12	22.95	-2.53	124.3
A Group	TF-12	0.124	11	0.512556	7	5.3	2.43	0.277179	-2.88	24.76	1.07	124.3
A Group	TF-13	0.124	9	0.512515	5	7.4	3.17	0.258973	-3.39	19.83	-2.75	124.3
A Group	TF-16	0.124	9	0.512625	6	4.8	1.63	0.205298	-0.39	17.4	1.59	124.3
A Group	TF-18	0.124	8	0.512524	8	7.7	2.6	0.204131	-2.34	23.57	1.62	124.3
A Group	TF-19	0.124	9	0.512539	6	4.8	2.12	0.267007	-3.05	24.65	-0.24	124.3
A Group	TF-20	0.124	12	0.512658	5	2.9	1.74	0.362737	-2.24	17.58	-1.94	124.3
A Group	TF-21	0.124	12	0.512605	7	4.3	2.5	0.351485	-3.10	23.34	-0.73	124.3
A Group	TF-22	0.124	12	0.512517	6	5.8	2.16	0.22514	-2.81	19.61	1.02	124.3
A Group	TF-23	0.124	12	0.512512	5	6.8	3.11	0.276489	-3.72	21.37	-2.7	124.3
A Group	TF-27	0.124	10	0.512572	9	5.1	2.62	0.310573	-3.09	23.77	0.61	124.3
A Group	TF-28	0.124	9	0.512539	9	6.7	2.73	0.24633	-2.72	20.21	1.09	124.3
A Group	TF-29	0.124	8	0.512584	7	5.5	3.64	0.400103	-4.28	23.83	0.94	124.3
A Group	TF-32	0.124	10	0.512573	8	7.5	3.7	0.298245	-2.88	18.51	-2.16	124.3
A Group	TF-38	0.124	12	0.51251	5	7	2.61	0.225407	-2.95	20.07	0.14	124.3
A Group	TF-43	0.124	8	0.512577	6	6.6	2.94	0.2693	-2.34	22.28	-3.33	124.3
A Group	TF-47	0.124	11	0.51252	7	6.9	3.01	0.263721	-3.37	23.8	-0.97	124.3
A Group	TF-57	0.124	8	0.512579	6	8.1	2.61	0.1948	-1.12	22.06	0.4	124.3
A Group	TF-58	0.124	10	0.512592	8	6.5	2.6	0.241821	-1.61	16.46	-1.94	124.3
A Group	TF-61	0.124	12	0.512601	6	6.9	1.54	0.134929	0.26	22.47	0.19	124.3
A Group	TF-64	0.124	8	0.512552	7	8.7	1.69	0.117435	-0.42	22.03	-0.19	124.3
A Group	TF-74	0.124	12	0.512607	9	6.6	3.64	0.333421	-2.77	16.51	1.85	124.3

(Continued on the following page)

TABLE 4 (Continued) Nd-C-O isotopic compositions of calcite from the Lucaogou Formation, Jimsar Sag, Junggar Basin.

Group	Sample	Age	2sm	$^{143}\text{Nd}/^{144}\text{Nd}$	2sm	Nd (ppm)	Sm (ppm)	$^{147}\text{Sm}/^{144}\text{Nd}$	$\epsilon\text{Nd}(t)$	$\delta^{18}\text{O}(\text{SMOW})$	$\delta^{13}\text{C}(\text{PDB})$	Age
A Group	TF-75	0.124	8	0.512641	6	4.6	2.28	0.299651	-1.58	23.79	-0.84	124.3
A Group	TF-78	0.124	9	0.512647	7	6.4	2.9	0.273941	-1.05	17.56	1.47	124.3
A Group	TF-81	0.124	8	0.512659	6	7.8	3.47	0.268953	-0.74	19.37	-1.86	124.3
A Group	TF-82	0.124	11	0.512515	6	5.3	2.47	0.281739	-3.75	20.34	-4.45	124.3
A Group	TF-86	0.124	12	0.512644	8	3.9	1.52	0.235623	-0.50	22.65	-1.42	124.3
A Group	TF-94	0.124	9	0.512631	6	8	2.53	0.191192	-0.05	18.81	-3.96	124.3
A Group	TF-96	0.124	12	0.512638	6	6.7	2.32	0.20934	-0.20	19.02	-3.18	124.3
A Group	TF-99	0.124	11	0.512591	8	5.3	2.06	0.234977	-1.52	21.46	-2.82	124.3
A Group	TF-102	0.124	10	0.51262	8	4.5	3.04	0.408412	-3.71	23.67	-3.04	124.3
A Group	TF-104	0.124	8	0.512633	5	5.4	2.18	0.244063	-0.85	24.09	-2.14	124.3
A Group	TF-110	0.124	9	0.512542	8	8.8	1.84	0.126405	-0.76	22.91	-1.17	124.3
A Group	TF-111	0.124	9	0.51252	6	7.7	2.39	0.187644	-2.16	19.79	-3.69	124.3
A Group	TF-112	0.124	12	0.512558	9	4.4	2.94	0.403948	-4.85	20.07	1.5	124.3
A Group	TF-117	0.124	12	0.512532	6	5.5	2.27	0.249512	-2.91	23.43	1.53	124.3
A Group	TF-123	0.124	8	0.512659	6	6.4	2.89	0.272998	-0.80	23.53	-1.92	124.3
A Group	TF-134	0.124	9	0.512518	7	7.3	2.19	0.181363	-2.10	21.34	-3.14	124.3
A Group	TF-135	0.124	9	0.512587	7	8.3	3.65	0.265857	-2.09	22.34	-1.28	124.3
A Group	TF-140	0.124	10	0.512521	5	5.9	2.19	0.224398	-2.72	21.64	2.29	124.3
A Group	TF-141	0.124	12	0.512591	9	3	1.73	0.348625	-3.33	21.91	-2.04	124.3
A Group	TF-143	0.124	9	0.512596	8	5	2.54	0.307113	-2.57	17.7	0.83	124.3
A Group	TF-152	0.124	9	0.512593	7	5.2	1.98	0.230195	-1.41	18.86	-1.64	124.3
A Group	TF-159	0.124	8	0.512627	8	8.3	3.56	0.259304	-1.21	17.73	-1.13	124.3
B Group	TF-14	0.189	11	0.512694	8	28.4	4.03	0.085789	3.78	19.65	-3.66	189

(Continued on the following page)

TABLE 4 (Continued) Nd-C-O isotopic compositions of calcite from the Lucaogou Formation, Jimsar Sag, Junggar Basin.

Group	Sample	Age	2sm	$^{143}\text{Nd}/^{144}\text{Nd}$	2sm	Nd (ppm)	Sm (ppm)	$^{147}\text{Sm}/^{144}\text{Nd}$	$\epsilon\text{Nd}(t)$	$\delta^{18}\text{O}(\text{SMOW})$	$\delta^{13}\text{C}(\text{PDB})$	Age
B Group	TF-24	0.189	11	0.512637	9	15	5.39	0.217238	-0.52	13.77	-2.49	189
B Group	TF-25	0.189	10	0.51279	9	16.3	3.82	0.141687	4.30	14.97	-5.04	189
B Group	TF-34	0.189	10	0.512703	7	15.4	4.62	0.181371	1.64	17.78	-4.26	189
B Group	TF-35	0.189	11	0.512736	9	27.3	5.05	0.111835	3.97	17.42	-2.93	189
B Group	TF-36	0.189	12	0.512654	9	18	3.96	0.133004	1.85	15.73	-3.98	189
B Group	TF-39	0.189	10	0.512712	5	24.3	5.9	0.146789	2.65	16.77	-4.57	189
B Group	TF-40	0.189	8	0.512663	9	15.8	3.73	0.142723	1.79	14.38	-4.9	189
B Group	TF-44	0.189	12	0.512666	6	23.9	4.79	0.121166	2.37	19.03	-2.59	189
B Group	TF-50	0.189	11	0.512775	5	32.1	4.48	0.084377	5.39	12.84	-6.67	189
B Group	TF-52	0.189	9	0.512783	7	38	5.25	0.083527	5.57	15.26	-4.38	189
B Group	TF-55	0.189	10	0.512755	7	19.5	5.47	0.169591	2.94	13.96	-4.28	189
B Group	TF-59	0.189	9	0.512721	9	35.1	4.67	0.080437	4.43	18.87	-5.41	189
B Group	TF-60	0.189	10	0.512662	6	17.8	3.5	0.118875	2.35	14.15	-3.51	189
B Group	TF-62	0.189	12	0.512818	5	30.2	4.62	0.092489	6.04	14.95	-7.36	189
B Group	TF-63	0.189	12	0.512648	5	18.3	5.28	0.174431	0.73	14.45	-4.99	189
B Group	TF-65	0.189	9	0.51267	5	26.4	3.76	0.086105	3.30	18.42	-5.98	189
B Group	TF-69	0.189	11	0.512788	8	16.1	5.47	0.205407	2.72	15.75	-3.92	189
B Group	TF-72	0.189	12	0.512714	5	31.1	3.41	0.066289	4.64	18.03	-2.15	189
B Group	TF-76	0.189	11	0.512722	8	25.3	3.74	0.089371	4.24	14.07	-6.53	189
B Group	TF-83	0.189	12	0.512777	6	17.3	4.04	0.141185	4.06	16.85	-4.64	189
B Group	TF-85	0.189	10	0.51276	6	24.8	3.75	0.091418	4.93	15.39	-5.81	189
B Group	TF-87	0.189	9	0.512689	6	28.7	4.15	0.08742	3.64	16.07	-6.21	189
B Group	TF-91	0.189	8	0.5128	7	27.9	5.64	0.122217	4.96	14.13	-5.49	189

(Continued on the following page)

TABLE 4 (Continued) Nd-C-O isotopic compositions of calcite from the Lucaogou Formation, Jimsar Sag, Junggar Basin.

Group	Sample	Age	2sm	$^{143}\text{Nd}/^{144}\text{Nd}$	2sm	Nd (ppm)	Sm (ppm)	$^{147}\text{Sm}/^{144}\text{Nd}$	$\epsilon\text{Nd}(t)$	$\delta^{18}\text{O}(\text{SMOW})$	$\delta^{13}\text{C}(\text{PDB})$	Age
B Group	TF-95	0.189	9	0.512763	5	24.2	4.54	0.113421	4.46	15.04	-3.89	189
B Group	TF-97	0.189	11	0.512768	6	22.4	3.85	0.103912	4.78	19.65	-2.25	189
B Group	TF-100	0.189	10	0.512757	7	23.1	4.28	0.112017	4.37	16.18	-2.05	189
B Group	TF-105	0.189	8	0.512759	7	36.7	5.41	0.089121	4.97	15.75	-3.81	189
B Group	TF-106	0.189	8	0.512731	9	39.5	5.47	0.083722	4.55	16.89	-6.64	189
B Group	TF-107	0.189	11	0.512662	8	30.7	5.67	0.111657	2.53	14.96	-6.59	189
B Group	TF-115	0.189	9	0.512803	8	26.8	3.32	0.074896	6.17	14.62	-5.95	189
B Group	TF-116	0.189	11	0.512778	7	29.4	3.1	0.063748	5.95	14	-5.24	189
B Group	TF-119	0.189	9	0.512773	6	39.7	3.04	0.046295	6.27	14.75	-6.96	189
B Group	TF-126	0.189	10	0.512779	8	36.2	4.61	0.076992	5.65	15.55	-3.66	189
B Group	TF-129	0.189	10	0.512768	7	18.2	3.25	0.10796	4.68	15.32	-4.14	189
B Group	TF-130	0.189	8	0.512711	8	38.9	7.82	0.121536	3.24	15.27	-5.99	189
B Group	TF-137	0.189	12	0.512758	9	24.9	5.9	0.143253	3.64	18.72	-4.75	189
B Group	TF-144	0.189	9	0.512676	8	28.3	4.04	0.086305	3.41	18.33	-6.3	189
B Group	TF-148	0.189	8	0.512712	9	17.6	4.11	0.141181	2.79	14.11	-3.8	189
B Group	TF-153	0.189	9	0.512675	7	37.3	5.22	0.084607	3.43	16.93	-2.53	189
B Group	TF-154	0.189	12	0.512784	8	29.5	3.61	0.073984	5.82	16.35	-2.16	189
B Group	TF-157	0.189	10	0.512775	7	31.3	3.08	0.059492	5.99	17.87	-4.44	189
B Group	TF-158	0.189	8	0.512706	7	24.8	3.93	0.095805	3.77	18.05	-5.05	189
C Group	TF-4	0.272	12	0.512932	6	32.5	4.73	0.087993	9.52	9.61	-5.2	272
C Group	TF-5	0.272	12	0.512973	9	32.2	7.64	0.143453	8.39	8.86	-4.56	272
C Group	TF-7	0.272	8	0.51294	8	27.5	7.37	0.162033	7.10	9.41	-5.76	272
C Group	TF-8	0.272	10	0.51296	6	32.3	4.89	0.091533	9.94	8.36	-5.38	272

(Continued on the following page)

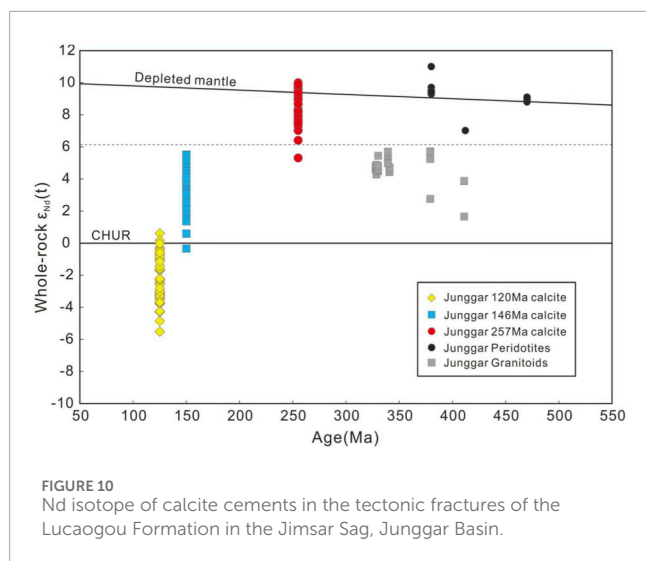
TABLE 4 (Continued) Nd-C-O isotopic compositions of calcite from the Lucaogou Formation, Jimsar Sag, Junggar Basin.

Group	Sample	Age	2sm	$^{143}\text{Nd}/^{144}\text{Nd}$	2sm	Nd (ppm)	Sm (ppm)	$^{147}\text{Sm}/^{144}\text{Nd}$	$\epsilon\text{Nd}(t)$	$\delta^{18}\text{O}(\text{SMOW})$	$\delta^{13}\text{C}(\text{PDB})$	Age
C Group	TF-9	0.272	8	0.512942	7	18.4	3.66	0.120263	8.59	5.41	-6.31	272
C Group	TF-11	0.272	12	0.512956	6	31.2	5.08	0.098442	9.62	9.64	-8.26	272
C Group	TF-15	0.272	10	0.512927	5	25.5	3.8	0.090097	9.35	11.13	-1.96	272
C Group	TF-26	0.272	9	0.512973	9	29.2	6.88	0.142455	8.42	9.44	-4.94	272
C Group	TF-30	0.272	11	0.512964	8	32.4	5.06	0.094423	9.92	14.44	-2.66	272
C Group	TF-31	0.272	8	0.512986	8	28.8	6.87	0.144224	8.62	9.72	-8.93	272
C Group	TF-41	0.272	9	0.512949	7	27.1	6.18	0.137876	8.12	8.81	-8.37	272
C Group	TF-48	0.272	11	0.512937	7	30.7	7.41	0.145932	7.60	13.63	-4.18	272
C Group	TF-49	0.272	10	0.512922	5	25	4.63	0.111972	8.49	11.25	-5.21	272
C Group	TF-53	0.272	8	0.512977	5	22.8	4.12	0.109254	9.66	8.84	-2.49	272
C Group	TF-54	0.272	12	0.512958	7	39.7	5.75	0.087569	10.04	12.4	-3.91	272
C Group	TF-56	0.272	9	0.512963	8	25.3	4.01	0.095829	9.85	8.96	-5.17	272
C Group	TF-66	0.272	10	0.512925	6	38.9	7.82	0.121542	8.21	6.2	-9.56	272
C Group	TF-67	0.272	9	0.512975	8	33.2	6.5	0.118372	9.30	10.28	-4.53	272
C Group	TF-68	0.272	11	0.512985	7	15.8	3.73	0.142734	8.65	10.89	-7.61	272
C Group	TF-73	0.272	9	0.512934	8	22.3	5.31	0.143966	7.61	9.06	-6.99	272
C Group	TF-88	0.272	9	0.512946	7	24.9	5.9	0.143259	7.87	4.51	-7.55	272
C Group	TF-89	0.272	10	0.512972	6	29.1	7.52	0.156242	7.93	9.19	-7.07	272
C Group	TF-90	0.272	9	0.512959	7	32.8	4.67	0.086082	10.11	8.93	-5.91	272
C Group	TF-92	0.272	11	0.512984	5	29.8	5.92	0.12011	9.42	8.11	-5.84	272
C Group	TF-98	0.272	8	0.512963	9	34.8	7.33	0.127349	8.75	9.43	-6.87	272
C Group	TF-101	0.272	9	0.512767	5	34.5	3.84	0.067292	7.02	17.49	-5.94	272
C Group	TF-108	0.272	8	0.512921	9	30.8	4.43	0.08696	9.34	14.86	-5.62	272

(Continued on the following page)

TABLE 4 (Continued) Nd-C-O isotopic compositions of calcite from the Lucaogou Formation, Jimsar Sag, Junggar Basin.

Group	Sample	Age	2sm	$^{143}\text{Nd}/^{144}\text{Nd}$	2sm	Nd (ppm)	Sm (ppm)	$^{147}\text{Sm}/^{144}\text{Nd}$	$\epsilon\text{Nd}(t)$	$\delta^{18}\text{O}(\text{SMOW})$	$\delta^{13}\text{C}(\text{PDB})$	Age
C Group	TF-109	0.272	10	0.512944	5	23.3	5.28	0.137009	8.05	9.16	-9.81	272
C Group	TF-113	0.272	12	0.512945	7	19.7	3.92	0.120307	8.65	11.73	-1.68	272
C Group	TF-114	0.272	8	0.512969	9	18.6	6.07	0.19731	6.44	14.84	-4.06	272
C Group	TF-120	0.272	8	0.512936	9	35.3	4.88	0.083582	9.75	11.83	-5.03	272
C Group	TF-121	0.272	10	0.512975	7	27.9	5.85	0.126772	9.01	8.2	-5.1	272
C Group	TF-122	0.272	12	0.512927	5	19.1	4.12	0.130416	7.95	9.15	-4.87	272
C Group	TF-124	0.272	12	0.512971	8	25.3	6.12	0.146253	8.25	13.46	-5.19	272
C Group	TF-125	0.272	12	0.512943	7	28	3.84	0.082917	9.91	9.65	-6.37	272
C Group	TF-132	0.272	9	0.51298	8	36.1	6.61	0.110705	9.66	15.72	-3.54	272
C Group	TF-139	0.272	8	0.512952	9	27	7.24	0.162123	7.33	9.71	-3.57	272
C Group	TF-142	0.272	12	0.512938	9	35.7	6.09	0.103138	9.11	5.97	-6.77	272
C Group	TF-146	0.272	10	0.512965	6	23.6	3.56	0.091203	10.05	11.3	-1.82	272
C Group	TF-147	0.272	8	0.512986	5	22.6	3.7	0.098985	10.19	4.54	-9.86	272
C Group	TF-149	0.272	11	0.512984	6	36.1	5.97	0.099987	10.12	14.21	-1.9	272
C Group	TF-155	0.272	8	0.512976	7	26.1	7.39	0.17119	7.48	11.44	-1.96	272



tectonic fracturing events. There are two episodes of deep fluid activities that are related to post-collision in the northern Xinjiang during the Permian, including the mantle-related fluid activity at 272.4 Ma and the crust-related fluid activity at 189.5 Ma. In addition, the third episode is related to the basin fluid activity at 124.3 Ma. In this study, we present the importance and necessity of combining geophysical and geochemical methods to constrain research on fluid activity episodes and fluid origins. Moreover, it is also critical to take regional tectonic evolution history and magmatism characteristics into account to accurately constrain deep fluid activities.

Data availability statement

The original contributions presented in the study are included in the article/supplementary material, further inquiries can be directed to the corresponding authors.

Author contributions

KD: Writing – original draft, Resources, Formal Analysis, Methodology, Visualization, Conceptualization. YX: Writing – review and editing, Supervision, Methodology, Resources, Conceptualization, Validation. TL: Supervision, Data curation, Methodology, Software, Conceptualization, Writing – review and editing, Investigation. HZ: Resources, Conceptualization, Project administration, Writing – review and editing, Methodology, Funding acquisition. PF: Supervision, Writing – review and editing, Software, Visualization, Validation.

HY: Software, Writing – review and editing, Resources, Formal Analysis, Methodology. SR: Conceptualization, Writing – review and editing, Validation, Methodology. CL: Methodology, Conceptualization, Writing – review and editing, Formal Analysis.

Funding

The author(s) declared that financial support was received for this work and/or its publication. This work was supported by the PetroChina Company Limited Science and Technology Project “Research on Key Technologies for Efficient Construction and Safe Operation of Underground Gas Storage” (Grant No. 2023YQX106). The funder was not involved in the study design, collection, analysis, interpretation of data, the writing of this article, or the decision to submit it for publication.

Conflict of interest

Authors KD, YX, TL, HZ, PF, SR, and CL were employed by CNPC Engineering Technology R&D Company Limited.

The remaining author(s) declared that this work was conducted in the absence of any commercial or financial relationships that could be construed as a potential conflict of interest.

Generative AI statement

The author(s) declared that generative AI was not used in the creation of this manuscript.

Any alternative text (alt text) provided alongside figures in this article has been generated by Frontiers with the support of artificial intelligence and reasonable efforts have been made to ensure accuracy, including review by the authors wherever possible. If you identify any issues, please contact us.

Publisher’s note

All claims expressed in this article are solely those of the authors and do not necessarily represent those of their affiliated organizations, or those of the publisher, the editors and the reviewers. Any product that may be evaluated in this article, or claim that may be made by its manufacturer, is not guaranteed or endorsed by the publisher.

References

- Agrinier, P., Destrienneville, C., Giunta, T., Bonifacie, M., Bardoux, G., Andre, J., et al. (2019). Strong impact of ion filtration on the isotopic composition of chlorine in young clay-rich oceanic sediment pore fluids. *Geochimica Cosmochimica Acta* 245, 525–541. doi:10.1016/j.gca.2018.11.013
- Anderson, R., Graham, C. M., Boyce, A. J., and Fallick, A. E. (2004). Metamorphic and basin fluids in quartz–carbonate–sulphide veins in the SW Scottish Highlands: a stable isotope and fluid inclusion study. *Geofluids* 4 (2), 169–185. doi:10.1111/j.1468-8115.2004.00080.x
- Balfour, N. J., Cummins, P. R., Pilia, S., and Love, D. (2015). Localization of intraplate deformation through fluid-assisted faulting in the lower-crust: the Flinders Ranges, South Australia. *Tectonophysics* 655, 97–106. doi:10.1016/j.tecto.2015.05.014
- Bau, M., and Möller, P. (1992). Rare earth element fractionation in metamorphogenic hydrothermal calcite, magnesite and siderite. *Mineralogy Petrology* 45 (3–4), 231–246. doi:10.1007/bf01163114
- Cai, C., Li, K., Li, H., and Zhang, B. (2008). Evidence for cross formational hot brine flow from integrated 87Sr/86Sr, REE and fluid inclusions of the Ordovician veins in Central Tarim, China. *Appl. Geochem.* 23 (8), 2226–2235. doi:10.1016/j.apgeochem.2008.03.009
- Chen, B., and Jahn, B. M. (2004). Genesis of post-collisional granitoids and basement nature of the Junggar Terrane, NW China: Nd–Sr isotope and trace element evidence. *J. Asian Earth Sci.* 23 (5), 691–703. doi:10.1016/s1367-9120(03)00118-4
- Davies, G. R., and Smith, L. B. (2006). Structurally controlled hydrothermal dolomite reservoir facies: an overview. *AAPG Bull.* 90 (11), 1641–1690. doi:10.1306/05220605164
- Dering, G. M., Micklethwaite, S., Cruden, A. R., Barnes, S. J., and Fiorentini, M. L. (2019). Evidence for dyke-parallel shear during syn-intrusion fracturing. *Earth Planet. Sci. Lett.* 507, 119–130. doi:10.1016/j.epsl.2018.10.024
- Elliott, G. M., Jackson, C. A. L., Gawthorpe, R. L., Wilson, P., Sharp, I. R., and Michelsen, L. (2017). Late syn-rift evolution of the Vingleia Fault Complex, Halten Terrace, offshore Mid-Norway; a test of rift basin tectono-stratigraphic models. *Basin Res.* 29, 465–487. doi:10.1111/bre.12158
- Foden, J., Barovich, K., Jane, M., and O'Halloran, G. (2001). Sr-isotopic evidence for Late Neoproterozoic rifting in the Adelaide Geosyncline at 586 Ma: implications for a Cu ore forming fluid flux. *Precambrian Res.* 106 (3–4), 291–308. doi:10.1016/s0301-9268(00)00132-7
- Gao, J. F., and Zhou, M. F. (2013). Generation and evolution of siliceous high magnesium basaltic magmas in the formation of the Permian Huangshandong intrusion (Xinjiang, NW China). *Lithos* 162, 128–139. doi:10.1016/j.lithos.2013.01.002
- Gao, Y. B., Li, K., Qian, B., Li, W. Y., Zheng, M. C., and Zhang, C. G. (2016). Trace elements, S, Pb, He, Ar and C isotopes of sphalerite in the Mayuan Pb–Zn deposit, at the northern margin of the Yangtze plate, China. *Acta Petrol. Sin.* 32 (1), 251–263.
- Goldstein, R. H. (2001). Fluid inclusions in sedimentary and diagenetic systems. *Lithos* 55 (1–4), 159–193. doi:10.1016/s0024-4937(00)00044-x
- Goyal, R., Tiwari, S., Tibbles, R. J., Anand, S., Ranjan, V., Sidharth, P., et al. (2016). Optimization of hydro-fracturing fluid for enhanced well performance in deep volcanic gas reservoir. In *Abu Dhabi International Petroleum Exhibition & Conference* (Society of Petroleum Engineers).
- Grandia, F., Cardellach, E., Canals, A., and Banks, D. A. (2003). Geochemistry of the fluids related to epigenetic carbonate-hosted Zn–Pb deposits in the Maestrat Basin, Eastern Spain: fluid inclusion and isotope (Cl, C, O, S, Sr) evidence. *Econ. Geol.* 98 (5), 933–954. doi:10.2113/gsecongeo.98.5.933
- Griffiths, L., Heap, M. J., Wang, F., Daval, D., Gilg, H. A., Baud, P., et al. (2016). Geothermal implications for fracture-filling hydrothermal precipitation. *Geothermics* 64, 235–245. doi:10.1016/j.geothermics.2016.06.006
- Hadlari, T., Midwinter, D., Galloway, J. M., Dewing, K., and Durbano, A. M. (2016). Mesozoic rift to post-rift tectonostratigraphy of the Sverdrup Basin, Canadian Arctic. *Mar. Petroleum Geol.* 76, 148–158. doi:10.1016/j.marpetgeo.2016.05.008
- Hart, N. R., Stockli, D. F., Lavier, L. L., and Hayman, N. W. (2017). Thermal evolution of a hyperextended rift basin, Mauléon Basin, western Pyrenees. *Tectonics* 36 (6), 1103–1128. doi:10.1002/2016tc004365
- Hazen, R. M., and Schiffries, C. M. (2013). Why deep carbon? *Rev. Mineralogy Geochem.* 75 (1), 1–6. doi:10.2138/rmg.2013.75.1
- Hergt, J. M., and Woodhead, J. D. (2007). A critical evaluation of recent models for Lau–Tonga arc–backarc basin magmatic evolution. *Chem. Geol.* 245 (1–2), 9–44. doi:10.1016/j.chemgeo.2007.07.022
- Hu, F., Zhou, C., Li, C., Xu, H., Zhou, F., and Si, Z. (2016). Water spectrum method of NMR logging for identifying fluids. *Petroleum Explor. Dev.* 43 (2), 268–276. doi:10.1016/s1876-3804(16)30030-1
- Immerzeel, W. W., Wanders, N., Lutz, A., Shea, J. M., and Bierkens, M. F. P. (2015). Reconciling high-altitude precipitation in the upper Indus basin with glacier mass balances and runoff. *Hydrology Earth Syst. Sci.* 19 (11), 4673–4687. doi:10.5194/hess-19-4673-2015
- Jin, X., Li, J., Hofstra, A. H., and Sui, J. (2017). Magmatic-hydrothermal origin of the early Triassic Laodou lode gold deposit in the Xiahe-Hezuo district, West Qinling orogen, China: implications for gold metallogeny. *Miner. Deposita* 52 (6), 883–902. doi:10.1007/s00126-016-0710-8
- Keith, B., Knechtges, P., Roberts, N. V., Elgeti, S., Behr, M., and Demkowicz, L. (2017). An ultraweak DPG method for viscoelastic fluids. *J. Newt. Fluid Mech.* 247, 107–122. doi:10.1016/j.jnnfm.2017.06.006
- Kent, A. J., Peate, D. W., Newman, S., Stolper, E. M., and Pearce, J. A. (2002). Chlorine in submarine glasses from the Lau Basin: seawater contamination and constraints on the composition of slab-derived fluids. *Earth Planet. Sci. Lett.* 202 (2), 361–377. doi:10.1016/s0012-821x(02)00786-0
- Kerrick, R., La Tour, T. E., and Willmore, L. (1984). Fluid participation in deep fault zones: evidence from geological, geochemical, and 18O/16O relations. *J. Geophys. Res. Solid Earth* 89 (B6), 4331–4343. doi:10.1029/jb089ib06p04331
- Kessel, R., Schmidt, M. W., Pettke, T., and Ulmer, P. (2005). Fluid and melt compositions coexisting with eclogite at high pressure and temperature. *Geochimica Cosmochimica Acta* 69 (10), A658.
- Kietäväinen, R., Ahonen, L., Niinikoski, P., Nykänen, H., and Kukkonen, I. T. (2017). Abiotic and biotic controls on methane formation down to 2.5 km depth within the Precambrian Fennoscandian Shield. *Geochimica Cosmochimica Acta* 202, 124–145. doi:10.1016/j.gca.2016.12.020
- Li, D., He, D., Santosh, M., and Ma, D. (2015). Tectonic framework of the northern Junggar Basin Part II: the island arc basin system of the western Luliang Uplift and its link with the West Junggar terrane. *Gondwana Res.* 27 (3), 1110–1130. doi:10.1016/j.gr.2014.08.019
- Li, H., Duan, H. T., Qin, Q. R., Zhao, T., Fan, C., and Luo, J. (2025). Characteristics and distribution of tectonic fracture networks in low permeability conglomerate reservoirs. *Sci. Rep.* 15, 5914. doi:10.1038/s41598-025-90458-6
- Liu, E., Zhao, J. X., Pan, S., Yan, D., Lu, J., Hao, S., et al. (2019). A new technology of basin fluid geochronology: *in-situ* U–Pb dating of calcite. *Earth Sci.* 44 (3), 698–712.
- Luo, A., He, J., Li, J., Gong, X., Cao, W., and Wu, Y. (2025). Experimental Study on the influence of water rock interaction on the mechanical characteristics and creep behavior of shale. *J. Geo Energy Environ.* 1 (2), 61–69. doi:10.62762/jgee.2025.256463
- Machel, H. G., and Lonnee, J. (2002). Hydrothermal dolomite—A product of poor definition and imagination. *Sediment. Geol.* 152 (3–4), 163–171. doi:10.1016/s0037-0738(02)00259-2
- Markl, G., and Bucher, K. (1998). Composition of fluids in the lower crust inferred from metamorphic salt in lower crustal rocks. *Nature* 391 (6669), 781–783. doi:10.1038/35836
- Montanari, D., Bonini, M., Corti, G., Agostini, A., and Del Ventisette, C. (2017). Forced folding above shallow magma intrusions: insights on supercritical fluid flow from analogue modelling. *J. Volcanol. Geotherm. Res.* 345, 67–80. doi:10.1016/j.jvolgeores.2017.07.022
- Peacock, J. R., Mangan, M. T., McPhee, D., and Ponce, D. A. (2015). Imaging the magmatic system of Mono Basin, California, with magnetotellurics in three dimensions. *J. Geophys. Res. Solid Earth* 120 (11), 7273–7289. doi:10.1002/2015jb012071
- Ruch, J., Wang, T., Xu, W., Hensch, M., and Jónsson, S. (2016). Oblique rift opening revealed by reoccurring magma injection in central Iceland. *Nat. Commun.* 7 (1), 1–7. doi:10.1038/ncomms12352
- Seewald, J. S., Reeves, E. P., Bach, W., Saccocia, P. J., Craddock, P. R., Walsh, E., et al. (2019). Geochemistry of hot-springs at the SuSu Knolls hydrothermal field, Eastern Manus Basin: advanced argillic alteration and vent fluid acidity. *Geochimica Cosmochimica Acta* 255, 25–48. doi:10.1016/j.gca.2019.03.034
- Shankland, T. J., and Ander, M. E. (1983). Electrical conductivity, temperatures, and fluids in the lower crust. *J. Geophys. Res. Solid Earth* 88 (B11), 9475–9484. doi:10.1029/jb088ib11p09475
- Sibson, R. H. (1994). Crustal stress, faulting and fluid flow. *Geol. Soc. Lond. Spec. Publ.* 78 (1), 69–84. doi:10.1144/gsl.sp.1994.078.01.07
- Sibuet, J. C., Deffontaines, B., Hsu, S. K., Thureau, N., Le Formal, J. P., and Liu, C. S. (1998). Okinawa trough backarc basin: early tectonic and magmatic evolution. *J. Geophys. Res. Solid Earth* 103 (B12), 30245–30267. doi:10.1029/98jb01823
- Smets, B., Delvaux, D., Ross, K. A., Poppe, S., Kervyn, M., d'Oreye, N., et al. (2016). The role of inherited crustal structures and magmatism in the development of rift segments: insights from the Kivu basin, western branch of the East African Rift. *Tectonophysics* 683, 62–76. doi:10.1016/j.tecto.2016.06.022
- Stasiuk, L. D., and Snowdon, L. R. (1997). Fluorescence micro-spectrometry of synthetic and natural hydrocarbon fluid inclusions: crude oil chemistry, density and application to petroleum migration. *Appl. Geochem.* 12 (3), 229–241. doi:10.1016/s0883-2927(96)00047-9
- Staudigel, P. T., Murray, S., Dunham, D. P., Frank, T. D., Fielding, C. R., and Swart, P. K. (2018). Cryogenic brines as diagenetic fluids: reconstructing the diagenetic history of the Victoria Land Basin using clumped isotopes. *Geochimica Cosmochimica Acta* 224, 154–170. doi:10.1016/j.gca.2018.01.002

- Stewart, B. W., Chapman, E. C., Capo, R. C., Johnson, J. D., Graney, J. R., Kirby, C. S., et al. (2015). Origin of brines, salts and carbonate from shales of the Marcellus Formation: evidence from geochemical and Sr isotope study of sequentially extracted fluids. *Appl. Geochem.* 60, 78–88. doi:10.1016/j.apgeochem.2015.01.004
- Stuart, F. M., Burnard, P. G., Taylor, R. P., and Turner, G. (1995). Resolving mantle and crustal contributions to ancient hydrothermal fluids: He-Ar isotopes in fluid inclusions from Dae Hwa W-Mo mineralisation, South Korea. *Geochimica Cosmochimica Acta* 59 (22), 4663–4673. doi:10.1016/0016-7037(95)00300-2
- Sverjensky, D. A. (1984). Europium redox equilibria in aqueous solution. *Earth Planet. Sci. Lett.* 67 (1), 70–78. doi:10.1016/0012-821x(84)90039-6
- Telling, J., Voglesonger, K., Sutcliffe, C. N., Lacrampe-Couloume, G., Edwards, E., and Sherwood Lollar, B. (2018). Bioenergetic constraints on microbial hydrogen utilization in Precambrian deep crustal fracture fluids. *Geomicrobiol. J.* 35 (2), 108–119. doi:10.1080/01490451.2017.1333176
- Turner, S., Handler, M., Bindeman, I., and Suzuki, K. (2009). New insights into the origin of O–Hf–Os isotope signatures in arc lavas from Tonga–Kermadec. *Chem. Geol.* 266 (3–4), 187–193. doi:10.1016/j.chemgeo.2009.05.027
- Walter, L. M., Stueber, A. M., and Huston, T. J. (1990). Br-Cl-Na systematics in Illinois basin fluids: constraints on fluid origin and evolution. *Geology* 18 (4), 315–318. doi:10.1130/0091-7613(1990)018<0315:bcnsii>2.3.co;2
- Wendler, J., Köster, J., Götze, J., Kasch, N., Zisser, N., Kley, J., et al. (2012). Carbonate diagenesis and feldspar alteration in fracture-related bleaching zones (Buntsandstein, central Germany): possible link to CO₂-influenced fluid–mineral reactions. *Int. J. Earth Sci.* 101 (1), 159–176. doi:10.1007/s00531-011-0671-1
- Winter, B. L., Johnson, C. M., and Clark, D. L. (1997). Strontium, neodymium, and lead isotope variations of authigenic and silicate sediment components from the Late Cenozoic Arctic Ocean: implications for sediment provenance and the source of trace metals in seawater. *Geochimica Cosmochimica Acta* 61 (19), 4181–4200. doi:10.1016/s0016-7037(97)00215-9
- Woodhead, J. D., Hergt, J. M., Davidson, J. P., and Eggins, S. M. (2001). Hafnium isotope evidence for conservative element mobility during subduction zone processes. *Earth Planet. Sci. Lett.* 192 (3), 331–346. doi:10.1016/s0012-821x(01)00453-8
- Xiao, W., Han, C., Yuan, C., Sun, M., Lin, S., Chen, H., et al. (2008). Middle Cambrian to Permian subduction-related accretionary orogenesis of Northern Xinjiang, NW China: implications for the tectonic evolution of central Asia. *J. Asian Earth Sci.* 32 (2–4), 102–117. doi:10.1016/j.jseas.2007.10.008
- Xue, S. C., Li, C., Qin, K. Z., and Tang, D. M. (2016). A non-plume model for the Permian protracted (266–286 Ma) basaltic magmatism in the Beishan–Tianshan region, Xinjiang, Western China. *Lithos* 256, 243–249. doi:10.1016/j.lithos.2016.04.018
- Zhang, M., O'Reilly, S. Y., and Chen, D. (1999). Location of Pacific and Indian mid-ocean ridge-type mantle in two time slices: evidence from Pb, Sr, and Nd isotopes for Cenozoic Australian basalts. *Geology* 27 (1), 39–42. doi:10.1130/0091-7613(1999)027<0039:lopaim>2.3.co;2
- Zhang, C., Santosh, M., Liu, L., Luo, Q., Zhang, X., and Liu, D. (2018). Early Silurian to Early Carboniferous ridge subduction in NW Junggar: evidence from geochronological, geochemical, and Sr-Nd-Hf isotopic data on alkali granites and adakites. *Lithos* 300, 314–329. doi:10.1016/j.lithos.2017.12.010
- Zhu, C. W., Wen, H. J., Zhang, Y. X., Fan, H. F., Fu, S. H., Xu, J., et al. (2013). Characteristics of Cd isotopic compositions and their genetic significance in the lead-zinc deposits of SW China. *Sci. China Earth Sci.* 56 (12), 2056–2065. doi:10.1007/s11430-013-4668-4